ELSEVIER

Journal of Environmental Management 85 (2007) 538–562

Journal of Environmental Management

www.elsevier.com/locate/jenvman

Future carbon balance of China's forests under climate change and increasing CO_2

W.M. Ju[a,*], J.M. Chen[a], D. Harvey[a], S. Wang[b]

[a]*Department of Geography, University of Toronto, 100 St. George St., Room 5047, Toronto, Ont., Canada M5S 3G3*

[b]*Key Laboratory of Ecosystem Network Observation and Modeling, The Synthesis Research Center, CERN, Institute of Geographic Sciences and Natural Resources Research, Datun Road No. 11A, Beijing 100101, PR China*

Received 8 November 2005; received in revised form 1 April 2006; accepted 16 April 2006
Available online 21 December 2006

Abstract

The possible response of the carbon (C) balance of China's forests to an increase in atmospheric CO_2 concentration and climate change was investigated through a series of simulations using the Integrated Terrestrial Ecosystem Carbon (InTEC) model, which explicitly represents the effects of climate, CO_2 concentration, and nitrogen deposition on future C sequestration by forests. Two climate change scenarios (CGCM2-A2 and -B2) were used to drive the model. Simulations showed that China's forests were a C sink in the 1990s, averaging 189 Tg C yr^{-1} (about 13% of the global total). This sink peaks around 2020 and then gradually declines to 33.5 Tg C yr^{-1} during 2091–2100 without climate and CO_2 changes. Effects of pure climate change of CGCM2-A2 and -B2 without allowing CO_2 effects on C assimilation in plants might reduce the average net primary productivity (NPP) of China's forests by 29% and 18% during 2091–2100, respectively. Total soil C stocks might decrease by 16% and 11% during this period. China's forests might broadly act as C sources during 2091–2100, with values of about 50 g C m^{-2} yr^{-1} under the moderate warming of CGCM2-B2 and 50–200 g C m^{-2} yr^{-1} under the warmer scenario of CGCM2-A2. An increase in CO_2 might broadly increase future C sequestration of China's forests. However, this CO_2 fertilization effect might decline with time. The CO_2 fertilization effects on NPP by the end of this century are 349.6 and 241.7 Tg C yr^{-1} under CGCM2-A2 and -B2 increase scenarios, respectively. These effects increase by 199.1 and 126.6 Tg C yr^{-1} in the first 50 years, and thereafter, by 150.5 and 115.1 Tg C yr^{-1} in the second 50 years under CGCM2-A2 and -B2 increase scenarios, respectively.

Under a CO_2 increase without climate change, the majority of China's forests would be C sinks during 2091–2100, ranging from 0 to 100 g C m^{-2} yr^{-1}. The positive effect of CO_2 fertilization on NPP and net ecosystem productivity would be exceeded by the negative effect of climate change after 2050. Under the CGCM2-A2 climate scenario and with direct CO_2 effects, China's forests may be a small C source of 7.6 Tg C yr^{-1} during 2091–2100. Most forests act as C sources of 0–40 g C m^{-2} yr^{-1}. Under the CGCM2-B2 climate scenario and with direct CO_2 effects, China's forests might be a small C sink of 10.5 Tg C yr^{-1} during 2091–2100, with C sequestration of most forests ranging from 0 to 40 g C m^{-2} yr^{-1}. Stand age structure plays a more dominant role in determining future C sequestration than CO_2 and climate change. The prediction of future C sequestration of China's forests is very sensitive to the Q_{10} value used to estimate maintenance respiration and to soil water availability and less sensitive to N deposition scenario.

The results are not yet comprehensive, as no forest disturbance data were available or predicted after 2001. However, the results indicate a range of possible responses of the C balance of China's forests to various scenarios of increase in CO_2 and climate change. These results could be useful for assessing measures to mitigate climate change through reforestation.

1. Introduction

Over half of the world's terrestrial organic soil and vegetation carbon (C) (~1150 Pg) is currently resident in forests (Prentice et al., 2001; Lal, 2005). These ecosystems play a significant role in the global C budget and in the variation of atmospheric CO_2 concentration. Small shifts in the balance between their photosynthesis and ecosystem respiration can result in large changes in C net exchange between forests and the atmosphere. The sizes of vegetation and soil C pools and fluxes in forests depend on

*Corresponding author. Tel./fax: 416 946 7715.
E-mail address: juw@geog.utoronto.ca (W.M. Ju).

0301-4797/$ - see front matter © 2006 Elsevier Ltd. All rights reserved.
doi:10.1016/j.jenvman.2006.04.028

climate (Apps et al., 2000; Black et al., 2000; Barr et al., 2002; Griffis et al., 2003; Wang et al., 2003), atmospheric CO_2 concentration (Chen et al., 2000a; Johnson et al., 2000; Alexandrov et al., 2003), nitrogen (N) deposition rate (Turunen et al., 2004), soil texture (Torn et al., 1997), drainage class (Rapalee et al., 1998), disturbance history (Sun et al., 2004), and stand age (Gower et al., 1996; Peltoniemi et al., 2004).

Climate affects photosynthesis and respiration processes in forests. Therefore, it is a major determinant of the C holding capacity and C budget of these ecosystems at various temporal scales. The future interaction between the C cycle and climate is a longstanding concern in climate change research. Several modelling studies simulate the possible impact of increasing atmospheric CO_2 concentration and future climate change on the terrestrial C cycle (Ludeke et al., 1995; King et al., 1997; Cao and Woodward, 1998; White et al., 2000; Cramer et al., 2001; Berthelot et al., 2002). It is commonly reported that the future increase in CO_2 concentration will enhance C sequestration by global terrestrial ecosystems, whereas climate change alone could reduce global terrestrial C stocks due to the reduction of global net primary productivity (NPP) (NPP reduction in the south exceeding NPP increase in the north) (Ludeke et al., 1995; Cao and Woodward 1998; Cramer et al., 2001; Berthelot et al., 2002). The combination of climate change and an increase in CO_2 concentration may enhance global terrestrial NPP and C sequestration during the 21th century (Ludeke et al., 1995; Cao and Woodward 1998; Cramer et al., 2001). The rate of increase of net ecosystem productivity (NEP) may begin to level off around 2030 (Cramer et al., 2001), although the current C sink at high latitudes could grow for a longer time than that in lower latitudes (White et al., 2000). The conclusions about the effect of climate change on global NPP and terrestrial C are not consistent. Anthony et al. (1997) reported that pure climate effects could increase global NPP by 10–15%.

China is the third largest country in the world and encompasses a broad range of climates, from tropical to subarctic/alpine and from rainforest to desert. Vegetation in China is diverse and species-rich (Fang et al., 2003). In the two most recent decades, China's biomes experienced a substantial increase in temperature, at a rate of $0.062\,K\,yr^{-1}$ from 1982 to 1998 (Fang et al., 2003). Model simulations, remote sensing monitoring, and forest inventory surveys show that China's terrestrial NPP increased significantly due to increases in temperature, precipitation and CO_2 concentration (Fang et al., 2003). The increase in NPP was spatially heterogeneous (Cao et al., 2003). The largest increases in NPP occurred in broad-leaf and needle-leaf mixed forests, located in Northeast China (Fang et al., 2003). A modeling experiment shows that future changes in climate with and without CO_2 direct physiological effects will result in an increase of C storage of 9% and 3%, respectively (Ni, 2000). China's forests occupied a total area of 229 Mha in 2001 (Wang et al., 2006, this issue) and are an important component of the global terrestrial C cycle. Recent estimates of the C balance in China's forests indicate that these ecosystems acted as a C sink during the past decades (Fang et al., 2001; Pan et al., 2004). Chinese biomes were projected to have a much greater increase in temperature than in the global mean and to have smaller or even no increases in precipitation (Giorgi et al., 2001). Therefore, it is important to predict the future C balance of China's forests under changing climate and increasing CO_2.

This study predicts the C balance in China's forests during the 21th century under climate change as simulated by the second version of the coupled atmosphere–ocean general circulation model (CGCM2) from the Canadian Climate Center, using radiative forcing from the SRES A2 and B2 emission scenarios. These climate change scenarios are used along with increasing atmospheric CO_2 concentration to drive the Integrated Terrestrial Ecosystem Carbon (InTEC) model (Chen et al., 2000b), which we describe here prior to presenting our results.

2. Model and simulation description

2.1. Model introduction

The InTEC C model is a process-based biogeochemical model designed to simulate annual C and N fluxes and pool sizes in forested ecosystems. It is driven by spatial data sets, including climate, soil texture, remotely sensed vegetation parameters (leaf area index (LAI) and land cover type), forest stand age, and N deposition data sets. It progressively simulates historical annual NPP for each pixel in terms of the initial value of NPP in the starting simulation year, age-dependent productivity of forest, and the combined effects on NPP of climate, CO_2 concentration, and N deposition (Chen et al., 2000b, 2003). These effects are simulated using a canopy-level photosynthesis module developed from Farquhar's instantaneous leaf-level biogeochemical model using a temporal and spatial scaling scheme (Chen et al., 2000b). The interannual variability of NPP is separated into contributions from changes in CO_2 concentration, growing season temperature, N content of foliage, growing season length, and LAI (Appendix Eqs. (A.10)–(A.41)). In the simulation, the initial NPP value of each pixel is iteratively tuned until the NPP value in a reference year (2001 in this study) simulated by InTEC at annual steps approaches that from the daily Boreal Ecosystems Productivity Simulator (BEPS) model (Liu et al., 2002). Soil C and N dynamics are simulated using the approaches of CENTURY (Parton et al., 1987), with some modifications (Ju and Chen, 2005).

The InTEC model includes two effects of fire on the C balance of forests. First, direct C release from forests to the atmosphere is estimated using the simplified model of Kasischke et al. (2000) (Appendix A.2), assuming that 100% of foliage C, 25% of stem C and 100% of surface litter C are burned, with the remaining biomass C transferred to soil C pools through the pathways embedded

in the model (Chen et al., 2003). Second, fire changes the age structure of forests and consequently forest productivity (Chen et al., 2003). The NPP of a forest is determined by the integrated effect of nondisturbance factors and by the normalized forest productivity, which changes with forest stand age (A.10). Climate affects NPP through its regulation of growing season length and photosynthesis rate. CO_2 is directly linked with intercellular CO_2 concentration and always has a direct positive effect on photosynthesis. The photosynthesis rate is positively related to the N content of foliage. N deposition normally enhances C sequestration prior to the maximum value of the N content of foliage being reached. No acidifying effects are included yet. The model assumes that all disturbances cause complete stand mortality and that the disturbed forest regenerates without cover-type change in the second year after a disturbance. Like other terrestrial biogeochemical models, InTEC uses a fixed land cover map in the whole simulation period. The incorporation of land use change and vegetation dynamics are tasks for further model improvement.

The InTEC model has been validated and used to (1) estimate the historical trend of the C balance in Canada's forests (Chen et al., 2000a); (2) to analyze the spatial patterns of current C sources and sinks in Canada's forests (Chen et al., 2003); (3) to simulate the spatial distribution of soil C stocks in Canada's forests and wetlands (Ju and Chen, 2005); and (4) to investigate hydrological effects on the C balance of Canada's forests and wetlands (Ju et al., 2006).

For the application of this model to China's forests, its soil carbon module was calibrated using measured soil organic C density and the decomposition rates of different soil C pools measured at several forested sites in China (Shao et al., 2006, this issue; Yang et al., 2006, this issue).

2.2. Model modification

The complete description of the InTEC model with modifications is presented in the appendix. The previous versions of the InTEC model do not explicitly include the effect on NPP of the change in canopy conductivity caused by the change in soil moisture availability. Canopy conductivity determines intercellular CO_2 concentration C_i and therefore has considerable influence on photosynthesis. The exclusion of interannual variability of canopy conductivity related to soil moisture availability could result in uncertainties in the simulated interannual variability of NPP. Canopy conductivity depends on maximum stomatal conductance, LAI, air temperature, incoming solar radiation, water vapor pressure deficit, and soil moisture (Jarvis, 1976).

Following the strategy of the TEM model (Pan et al., 1998), the intercellular CO_2 concentration C_i is linked with the atmospheric CO_2 concentration C_a as

$$C_i = \alpha C_a, \tag{1}$$

where α is a dimensionless multiplier that accounts for changes in canopy conductivity to CO_2 resulting from changes in soil moisture availability.

According to Eq (1), we replace the variable C_i in the canopy photosynthesis model with α to account for the effect of soil moisture availability on NPP (A.25, A.27, and A.36). The multiplier α is a function of the ratio of actual evapotranspiration to potential evapotranspiration (Pan et al., 1998) (A.65).

Elevated CO_2 can reduce transpiration (Tricker et al., 2005) and therefore increase water use efficiency, which will enhance C assimilation under dry conditions. However, the plant response to elevated CO_2 varies by species, and most experimental data come from pot or chamber experiments and are thus not well suited for models of mature ecosystems. The InTEC model has not included this mechanism yet. This exclusion of reduced transpiration caused by increase in CO_2 possibly underestimates NPP in the coupled runs.

Previously, InTEC assumed that the ratio of NPP to GPP is constant as climate and N status change (Chen et al., 2000b). This implies that climate warming generally has positive effects on NPP, which is not true in some cases. To remove this assumption, the effect of temperature on autotrophic respiration is added in this study. Interannual variability of GPP is first calculated using a modified algorithm (A.18–A.41). The historical values of NPP are progressively computed from the interannual variations of GPP and autotrophic respiration, and the ratio of respiration to GPP (A.11–A.17). The reduction of Q_{10} (the sensitivity of maintenance respiration to temperature) with increasing temperature is not included in this study. This may overestimate the negative effect of climate warming on NPP.

2.3. Data used

This study uses a control and two projected future climates (A2 and B2) from the second version of the first generation of the Canadian coupled general circulation model (CGCM2) (Gough and Leung, 2002). The outputs of CGCM2 are at a $3.75^\circ \times 3.75^\circ$ spatial resolution. To adjust for climate model bias, the additive departures for temperature and multiplicative departures for precipitation during 2002–2100 relative to the 1990–2001 projected mean climates were interpolated to 1 km resolution in the same way for historical climate data. The interpolated anomalies were applied to the historical climatology observed during 1990–2001 to produce time series of future climates during 2002–2100 for each pixel. This strategy of downscaling climate model outputs preserved interannual variability of the projected climates, while simultaneously forcing their spatial patterns to be in agreement with recent observations (Cramer et al., 2001).

In the control run of CGCM2, current greenhouse gas levels are used. Therefore, projected future climates do not depart from contemporary ones (Fig. 1). In the A2 run,

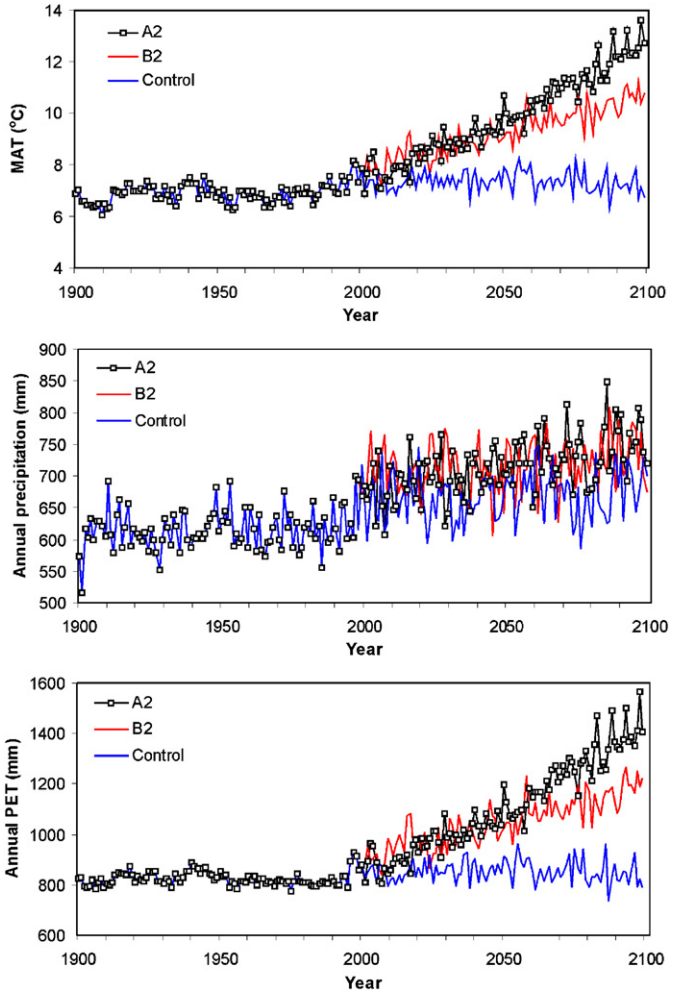

Fig. 1. Time series of mean annual temperature (MAT), annual precipitation, annual potential evopotranspiration (PET) used in simulations. Values prior to 2002 are interpolated and calculated from historical observations. Projected climates from control, A2 and B2 runs of CGCM2 are used for the period from 2002 to 2100.

CO_2 increases from 350 in 1990 to 850 ppmv in 2100. This is a warming scenario. On the average, mean annual temperature (MAT) in China's forested areas increases by 5 K during 2001–2100, whereas precipitation increases by only about 10%. PET almost doubles by 2100 (Fig. 1). In the B2 run, CO_2 increases from 350 in 1990 to 600 ppmv in 2100. The warming in this scenario is moderate, with an increase in MAT of about 3.0 K during 2001–2100. This scenario also projects a smaller increase in the total precipitation than does CGCM2-A2 (Fig. 1). More detailed descriptions of the CGCM2 model and corresponding runs are found in Flato and Boer (2001). The changes in temperature and precipitation projected by CGCM2-A2 and CGCM2-B2 are not spatially uniform (Fig. 2). Increases in temperature occur in all areas, especially in Central, North and Northwest China, while some coastal and southwestern areas experience smaller temperature increases during the following 100 years. The changes in precipitation are more spatially heterogeneous with increases in precipitation projected by CGCM2-A2 mainly the southern part of Northwest, North, and the southwestern part of Northeast China. In regions such as the northern part of Northwest, most of Southwest, and the southwestern part of Southeast China, precipitation will decrease slightly during the following 100 years (Fig. 2b). The CGCM2-B2 scenario projects smaller increases or even larger decreases in precipitation for most regions of China than does the CGCM2-A2 scenario.

In all simulations, we drive the model with the same spatial data sets of LAI, land over, stand age, soil texture, reference NPP and N deposition in 2001, and historical climate. Historical climate data from 1901 to 1998 was developed from the 0.5° global data set established by the UK Climate Research Unit from available station observations (New et al., 1999, 2000). Meteorological data at 743 stations of the National Meteorological Administration in China were used for 1999–2001 since the global data set is only available prior to 1999. Historical climate data were interpolated to 1 km resolution using a bilinear interpolation scheme. All simulations used the same method to initialize biomass and soil C pools (Ju and Chen, 2005). The future N deposition rate was estimated from the measured N deposition rate in 2001 (Wang et al., 2006, this issue) and estimated future national greenhouse gas emissions under the assumption that the national emission will be doubled during 2001–2100. Soil texture data were interpolated from 5405 soil profiles of the second national soil survey taken during the 1980s. A map of stand age in 2001 was constructed based on inventory data recorded during 1989–1993 in 32 provinces (Wang et al., 2006, this issue). NPP in 2001 simulated at a daily time step using the BEPS model (Feng et al., 2006, this issue) was used to tune the initial NPP value. Maps of LAI and land cover were derived from remote sensing data (Feng et al., 2006, this issue).

2.4. Simulations performed

In order to investigate the response of the C cycle in China's forests to climate change and increasing CO_2, we conducted seven model simulations (Table 1). In simulation 1, contemporary CO_2 concentration and climates from the control run of CGCM2 were used to drive the model. The changes in C balance are due to the change of stand age and N input from atmospheric deposition. In simulations 2 and 5, the A2 and B2 CO_2 concentration scenarios and the corresponding climates as projected by CGCM2 were used to evaluate the response of the C balance in China's forests to the integrated effect of changing climate and increasing CO_2. In simulations 3 and 6 the model is driven using projected climate alone. These runs are to investigate how pure climate change could impact the future C balance of China's forests. In simulations 4 and 7, the model is driven by the changing CO_2 concentration alone (using the control run climate). These simulations are to predict the responses of the future C balance of China's forests to different levels of CO_2 concentration.

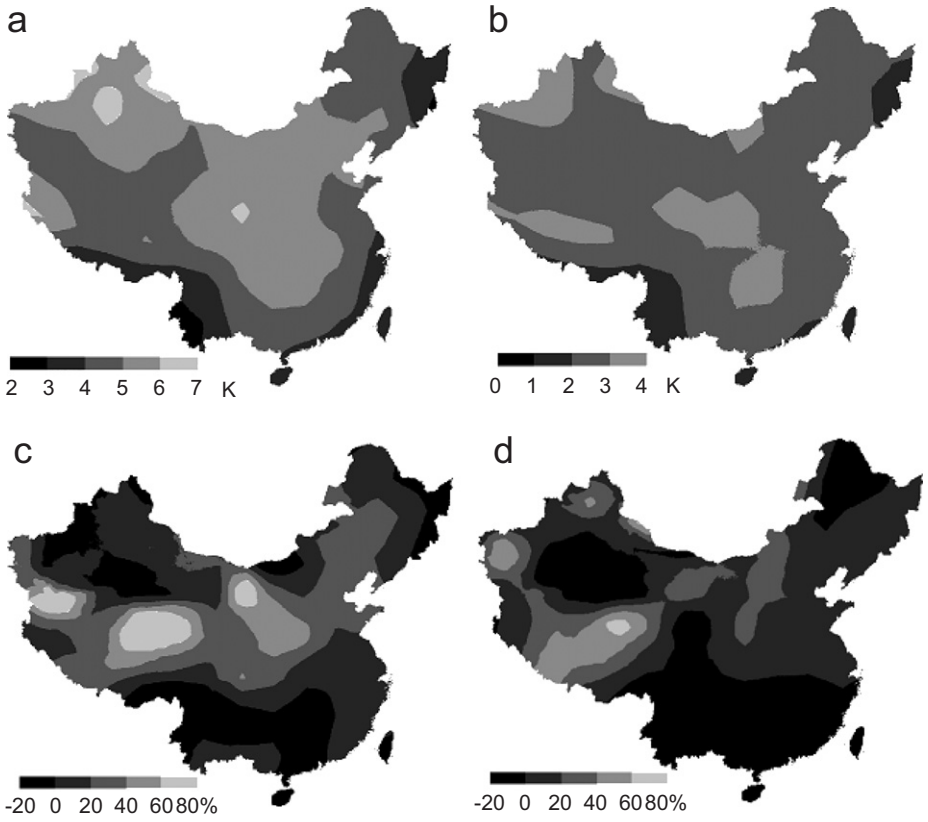

Fig. 2. Spatial distribution of changes in mean annual temperature (MAT). (upper panel). Values are the difference of MAT during 2091 compared with that during 2001–2010: (a) CGCM2-A2; (b) CGCM2-B2. The change in annual total precipitation during 2091–2100 relative to that during 2001–2010 (lower panel): (c) CGCM2-A2; (d) CGCM2-B2.

Table 1
Description of seven simulations performed

Run no.	Run name	Future climate	Future CO_2 (ppmv)
1	Baseline	CGCM2-control	371 during 2001–2100
2	CGCM2-A2 coupled	CGCM2-A2	From 371 to 850 during 2001–2100
3	CGCM2-A2 climate	CGCM2-A2	371 during 2001–2100
4	CGCM2-A2 CO_2 fertilization	CGCM2-control	From 371 to 850 during 2001–2100
5	CGCM2-B2 coupled	CGCM2-B2	From 371 to 600 during 2001–2100
6	CGCM2-B2 climate	CGCM2-B2	371 during 2001–2100
7	CGCM2-B2 CO_2 fertilization	CGCM2-control	From 371 to 600 during 2001–2100

3. Results and discussions

3.1. Response of NPP to climate change and increasing CO_2

Simulated series of historical and future NPP are shown in Fig. 3. NPP of China's forests increases from 951.4 Tg C yr^{-1} in 1901 to 1131.0 Tg C yr^{-1} in 2001 according to our simulation. The quick increase in NPP of China's forests during the 1980s and 1990s is possibly due to the effect of climate change and forest regrowth acting together (Fang et al., 2003). When the model is driven by the contemporary CO_2 concentration and the CGCM2 control climate, the mean NPP of China's forest increases to 1252.5 Tg C yr^{-1} during 2091–2100, 121.5 Tg C yr^{-1} higher than the value in 2001. This increase in NPP is mainly due to the effects of N input from atmospheric deposition and changes in forest productivity related to the change of stand age structure. The increase of CO_2 concentration will enhance the NPP of China's forests while pure climate warming has a considerable negative effect on NPP. The CGCM2-A2 CO_2 fertilization run yields the highest NPP (Fig. 3a). In this run, the average NPP during 2091–2100 increases to 1602.1 Tg C yr^{-1}, 362 Tg C yr^{-1} higher than the value during 2001–2010 (Table 2). The CO_2 increase in the B2 fertilization run is smaller and so leads to a smaller increase in NPP (Fig. 3b); the average NPP during

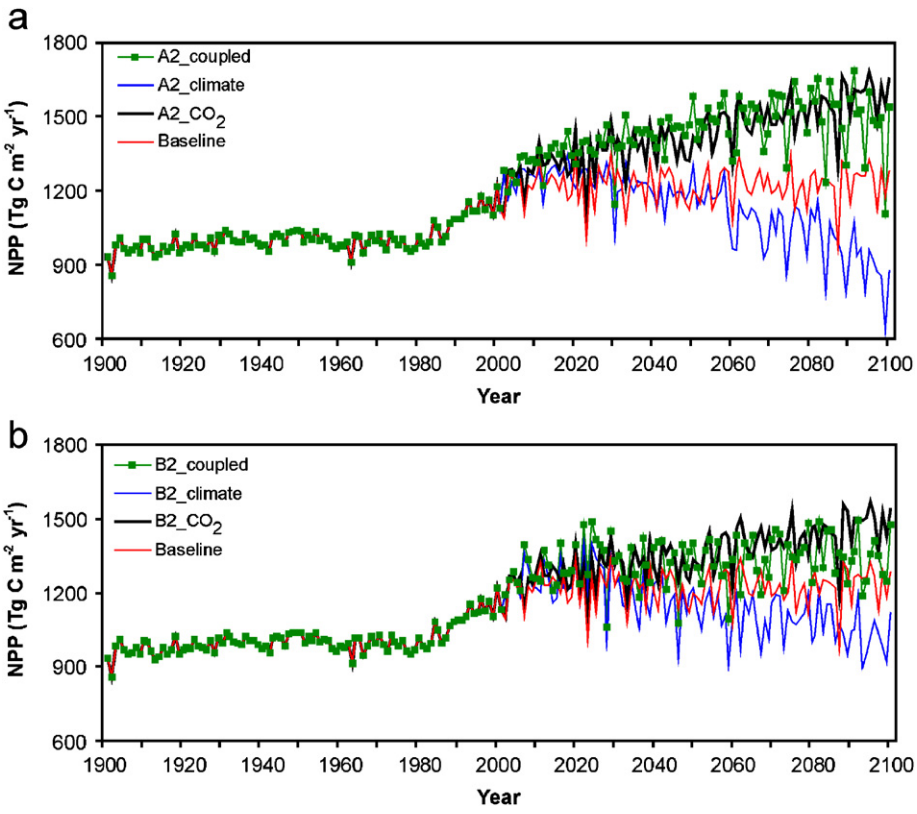

Fig. 3. Time series of NPP output from different simulation experiments. All simulations were driven by same spatial and historical climate data sets and produced same NPP values for the period from 1901 to 2001. The difference in NPP during 2002–2100 is due to different future climate and CO_2 concentration data sets used.

Table 2
Simulated mean NPP of China's forests under different climate and CO_2 change scenarios (Tg C yr^{-1})

	2001–2100	2001–2010	2045–2054	2091–2100
A2 Climate and CO_2	1432.4	1274.2	1472.1	1470.5
A2 Climate	1128.1	1233.9	1190.1	889.4
A2 CO_2	1425.0	1240.1	1390.6	1602.1
B2 Climate and CO_2	1323.0	1255.2	1323.1	1341.3
B2 Climate	1148.2	1233.5	1141.7	1025.4
B2 CO_2	1354.3	1219.2	1324.9	1494.2
Baseline	1221.3	1198.8	1197.5	1252.5

Values in this table are the NPP simulated using different scenarios of climate and CO_2 concentration changes in comparison with that simulated in the baseline run using contemporary CO_2 concentration (371 ppmv) and climate from the control run of CGCM2.

2091–2100 increases to only 1494.2 Tg C yr^{-1}, 107.9 Tg C yr^{-1} lower than the value in the A2 CO_2 fertilization run (Table 2).

The values of the β factor ($\beta = [NPP_{C_a}/NPP_0 - 1)]/\ln(Ca/C_a^0)$, where C_a is ambient CO_2 concentration, C_a^0 is baseline concentration of CO_2) (Alexandrov et al., 2003) for the future CO_2 enrichment of NPP are 0.35 and 0.42 for the CGCM2-A2 and -B2 CO_2 fertilization scenarios, respectively. They are much higher than the value of 0.14 simulated by Chen et al. (2000a) for Canada's forests during 1896–1996, but are in the lower part of the range of 0.3–0.6 in studies of the response of global NPP to future CO_2 fertilization (Cao and Woodward, 1998; Cramer et al., 2001). When CO_2 concentration increases to 550 ppmv, simulated NPP will increase by 13% under the CGCM2-A2 increase scenario and by 16% under the CGCM2-B2 increase scenario, only about 57% and 70% of the value of Norby et al. (2005) derived from FACE experiments across a broad range of conditions. Their stimulation of NPP by elevated CO_2 ($\approx$550 ppmv) is at the median of 23$\pm$2%. Our simulated CO_2 fertilization enhancement of NPP during 2001–2100 is 28% for the CGCM2-A2 CO_2 increase scenario and 19% for the CGCM2-B2 CO_2 increase scenario, respectively. Both are smaller than a simulated increase of about 52% in global NPP due to a gradual CO_2 increase to 795 ppmv in 2100 obtained by Cramer et al. (2001). A coupled climate–carbon cycle model predicts that CO_2 fertilization without climate change will increase NPP in 30°N–50°N by 60% in 2100 under the A2 scenario (Berthelot et al., 2002). This projected CO_2 fertilization effect is much stronger than our results (28% for the CGCM2-A2 CO_2 increase scenario and 19% for the CGCM2-B2 CO_2 increase scenario).

Our model predicts that the CO_2 fertilization effects on NPP by the end of this century are 349.6 and 241.7 Tg

C yr^{-1} under CGCM2-A2 and -B2 increase scenarios, respectively. These effects increase by 199.1 and 126.6 Tg C yr^{-1} in the first 50 years, and thereafter, by 150.5 and 115.1 Tg C yr^{-1} in the second 50 years under CGCM2-A2 and -B2 increase scenarios, respectively (Table 3). This early rise and subsequent decline of the CO_2 enhancement of NPP is consistent with some other recent findings (Oren et al., 2001; Marissink et al., 2002; Rasse et al., 2005). After long-term exposure to elevated CO_2, forests produce litter with a high C/N ratio (Cotrufo and Ineson, 1996; Sadowsky and Schortemeyer, 1997), which increases immobilization and reduces the amount of N available for the uptake by forests. The positive effect of an increase in CO_2 on NPP is partially offset by the reduced N content of foliage. Through this mechanism, the benefit of NPP from CO_2 fertilization will gradually decline with time.

Pure climate changes projected by CGCM2-A2 and -B2 cause considerable reductions in NPP of China's forests according to our simulations. The warmer climate of CGCM2-A2 will possibly result in a decrease of about 29% in decadal average NPP (2091–2100) by the end of this century. The moderate warming of CGCM2-B2 has a less negative influence on NPP, reducing NPP by about 18% after 100 years (Table 3). Pure climate change will mainly negatively impact NPP in the late half of this century (Fig. 3 and Table 3), when the positive effect of warming on transport and rubisco activity is exceeded by the combination of negative effects of reduced canopy conductance on GPP due to water stress (Fig. 4) and enhanced maintenance respiration. During the first 50 years of this century, the negative effect of climate change on NPP is relatively small.

Table 3
Effects of different climate and CO_2 change scenarios on mean NPP of China's forests (Tg C yr^{-1})

	2001–2100	2001–2010	2045–2054	2091–2100
A2 Climate and CO_2	211.1	75.5	274.6	218.0
A2 Climate	−93.2	35.1	−7.4	−363.1
A2 CO_2	203.6	41.3	199.1	349.6
B2 Climate and CO_2	101.7	56.4	125.6	88.8
B2 Climate	−73.1	34.8	−55.8	−227.1
B2 CO_2	133.0	20.4	126.6	241.7

Values in this table are differences between the NPP simulated using different scenarios of climate and CO_2 concentration changes and that simulated using contemporary CO_2 concentration (371 ppmv) and climate from the control run of CGCM2.

The coupled effect of CO_2 and climate change will largely enhance NPP before 2050. In the CGCM2-A2 coupled run, average NPP will increase from 1274.2 Tg C yr^{-1} in 2001–2010 to 1472.1 Tg C yr^{-1} during 2045–2054, 1526.6 Tg C yr^{-1} in the 2070s and then decrease to 1470.5 Tg C yr^{-1} in 2090–2100 due to the positive effect of CO_2 fertilization being exceeded by the negative effect of climate change. In the CGCM2-B2 coupled run, the change of NPP shows a similar temporal pattern but with a smaller magnitude. The simulated response of NPP to the combined effect of climate change and the increase in CO_2 is within the range of results obtained at the global scale (Cao and Woodward, 1998; Cramer et al., 2001; Berthelot et al., 2002).

NPP will increase in most forests in China during the next 100 years due to increasing CO_2 and changes in climate and stand age, especially in Southeast China (Fig. 5). In these regions, NPP will increase considerably due to the positive effects of increasing CO_2, large N deposition, and the increasing productivity related to stand age structure. These positive effects on NPP exceed a small negative effect from climate change. In the CGCM2-A2 coupled run, NPP of these forests will increase by above 200 g C m^{-2} yr^{-1} in 100 years. In addition to the contribution from increasing CO_2, two other factors are possible candidates explaining such big increases in NPP here. First, most stands in these areas are currently immature and will become more productive in the future. Second, measured N deposition is much higher here than in other regions due to heavy industrialization. This model assumes NPP to linearly increase with the N content of foliage and does

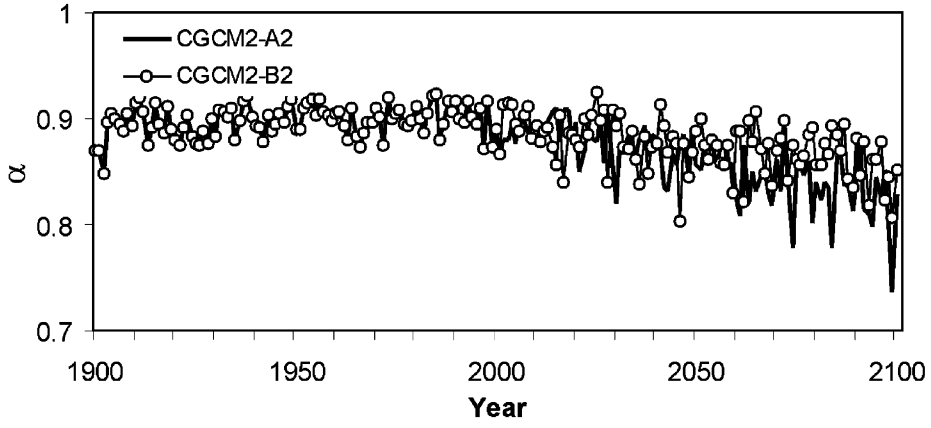

Fig. 4. Time series of the mean of growing season relative canopy conductivity to CO_2 α, which is related to soil moisture availability and calculated using Eq. (2). A small α value indicates that canopy conductivity to CO_2 is limited by soil moisture.

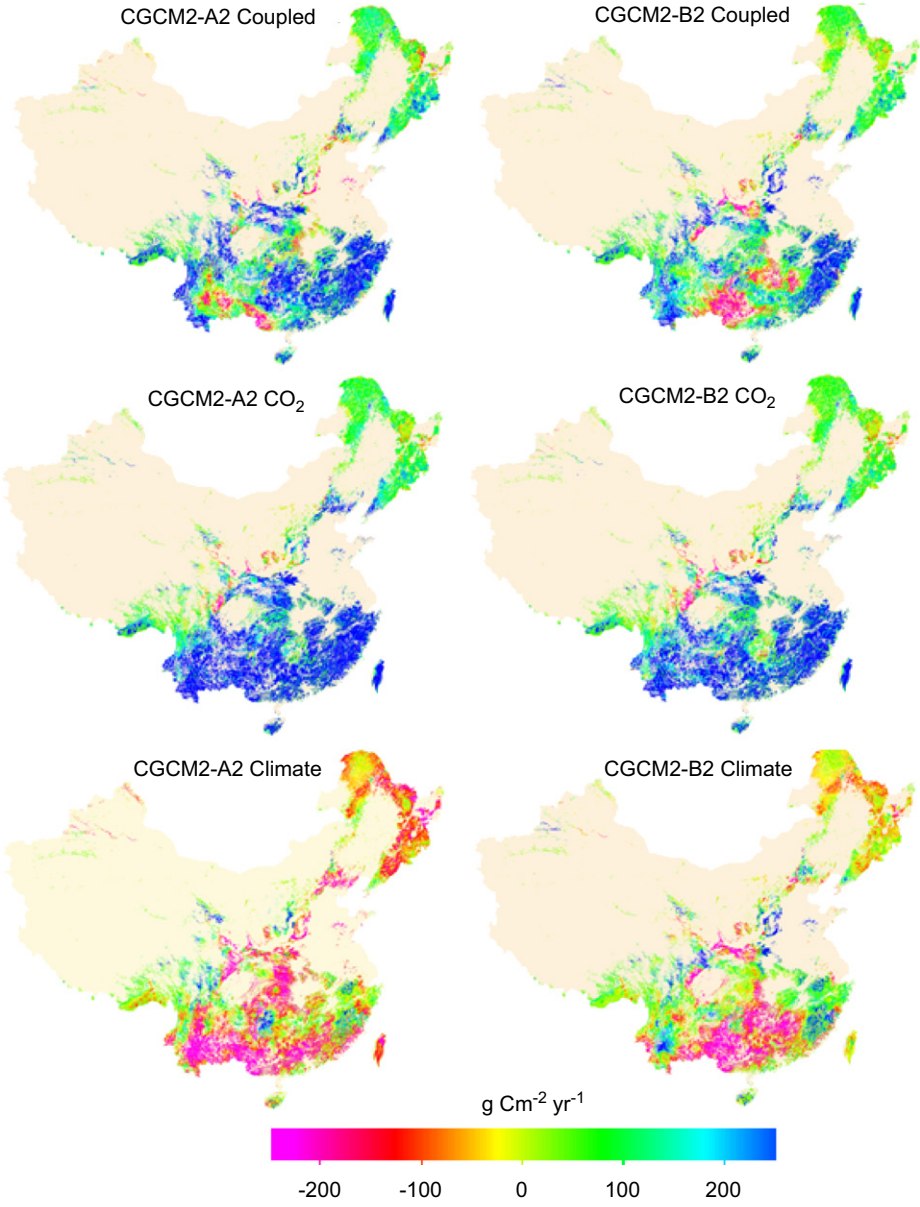

Fig. 5. Departure of average NPP during 2091–2100 from values during 1991–2000 under different climate change and increase in CO_2 scenarios. Positive values represent NPP increase, and vice versa.

not consider the effect of acidification. The increase of NPP in Northeast China will be relatively small, normally less than 100 g C m^{-2} yr^{-1} in 100 years. NPP of some forests in Southwest China will decrease by about 200 g C m^{-2} yr^{-1} in the coupled runs. NPP widely increases in the CO_2 fertilization runs. In this century, NPP of most forests in regions south of the Yangtze River will increase by above 200 g C m^{-2} yr^{-1} due to CO_2 fertilization. NPP of old forests in Northeast China will increase by about 100 g C m^{-2} yr^{-1}. Pure climate change alone will cause reductions in NPP for most of China's forests except forests in the western part of Southwest and the northern part of Southeast China. Here, NPP will have small increases.

The combined effect of climate change and CO_2 fertilization will increase forest NPP in all climate zones (Fig. 6), especially in the plateau temperate and plateau frigid zones (Table 4). Mean NPP values during 2091–2100 in the CGCM2-A2 coupled run are 88% and 63% higher than those in the baseline run for these two climate zones. In the CGCM2-B2 coupled run, these numbers are 71% and 32%, respectively. Climate without a corresponding increase in CO_2 will cause reductions in NPP in all climate zones except plateau temperate and plateau frigid zones. Climate change will increase NPP in these areas.

3.2. *Response of carbon storage to climate change and increasing CO_2*

The simulated total C stock in China's forests varies annually between 28.9 and 34.5 Pg C during 1900–2001,

with 11.6–17.4 Pg C in vegetation and 16.8–17.7 Pg C in soils, respectively. The total ecosystem, vegetation, and soil C stocks are in the range of recent published results (Pan et al., 2004; Wang et al., 2004). An increase in CO_2 will increase the total C stock in vegetation during 2001–2100, while climate change alone will reduce vegetation C after 2050 (Fig. 7). As expected, similar to NPP, the vegetation C stock has the highest value in the CGCM2-A2 CO_2 fertilization run in 2091–2100. The increase of total vegetation C amounts to 12.6 Pg C from 2001 to 2100 (to be compared to increases of 11.0 Pg C in the CGCM2-B2 CO_2 fertilization run and 7.6 Pg C in the baseline run). The increases of the vegetation C stock are 3.9 and 5.1 Pg C during 2001–2100 in the CGCM2-A2 and -B2 climate change runs, respectively. The decreases of vegetation C caused by pure climate change of CGCM2-A2 and -B2 are 3.7 and 2.5 Pg C, respectively, mainly in the second half of this century. The combined effect of climate change and increasing CO_2 will increase the vegetation C stock by 4.3 and 2.0 Pg C in 2100 under the CGCM2-A2 and -B2 scenarios, respectively.

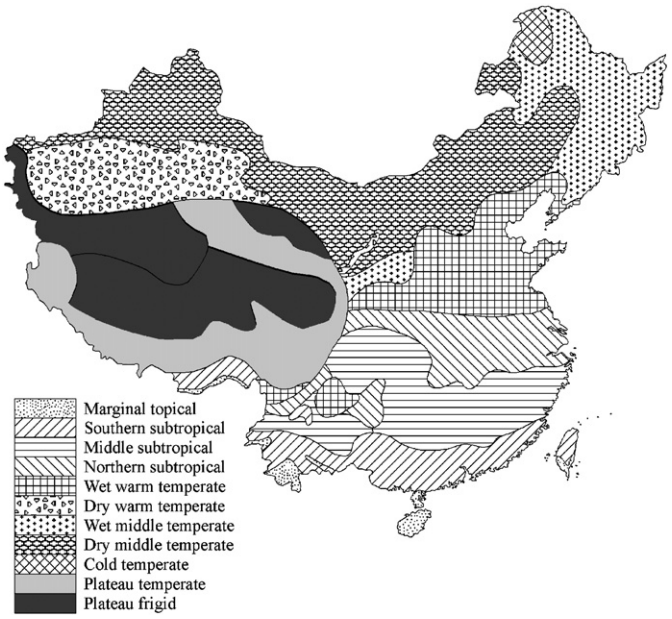

Fig. 6. Distribution of different climate zones in China.

Climate change has a negative effect on the soil C stock due to an enhancement in heterotrophic respiration and a decrease in litter input resulting from reduced NPP for these cases when NPP decreases. The soil C stock increases by 3.3 Pg C between 2001 and 2100 in the baseline run, but by only 0.1 and 1.0 Pg C from 2001 to 2100 in the CGCM2-A2 and -B2 climate impact runs, respectively (Fig. 8). Pure climate change of CGCM2-A2 and -B2 will reduce soil C stock by 3.2 and 2.3 Pg C in 100 years, respectively. In addition to the positive effect on NPP, CO_2 fertilization also has the possibility to reduce heterotrophic respiration by increasing the C/N ratios of the litter and soil C pools (Potter et al., 1993; Cao and Woodward, 1998). In addition, when foliage and fine roots have larger C/N ratios, more foliage and fine root litter will be partitioned into structural litter pools and less into metabolic litter pools. Structural litter pools have slower decomposition rates than metabolic litter pools. In the CO_2 fertilization runs, the overall temporal trends in heterotrophic respiration are dominated by the increasing NPP and therefore mirror the NPP changes with a time lag of about 20 years. The increase in soil C stock due to the increase in CO_2 amounts to 2.8 and 1.8 Pg C (equal to soil C stock in the fertilization runs minus the value in the baseline run) in 2100 under CGCM2-A2 and -B2 CO_2 increase scenarios, respectively.

The total C stock of China's forests is enhanced by the increase in CO_2 (Fig. 9) through its stimulation on NPP and its indirect effect on decreasing soil C decomposition. The largest increase is for the CGCM2-A2 CO_2 fertilization run, amounting to 18.6 Pg C from 2001 to 2100. The enhancement effect of CGCM2-A2 CO_2 fertilization in 100

Table 4
Simulated mean NPP of China's forests during 2091–2100 in different climate zones under different climate and CO_2 change scenarios (Tg C yr^{-1})

Climate zone	Simulations						
	Baseline	CGCM2-A2 coupled	CGCM2-A2 climate	CGCM2-A2 CO_2	CGCM2-B2 Coupled	CGCM2-B2 climate	CGCM2-B2 CO_2
Marginal tropical	46.00	52.84	33.22	58.53	51.68	38.53	54.96
Southern tropical	285.06	292.91	153.98	368.94	264.89	194.72	344.53
Middle tropical	421.17	509.34	311.89	550.82	433.16	318.32	510.18
Northern tropical	145.46	164.32	89.72	182.63	158.29	120.01	170.11
Wet warm temperate	84.53	97.62	53.27	110.57	96.13	76.14	100.76
Dry warm temperate	0.12	0.04	0.01	0.15	0.14	0.04	0.13
Wet middle temperate	182.61	218.86	151.69	217.35	211.10	173.32	207.81
Dry middle temperate	16.50	20.92	11.69	22.16	22.80	18.98	19.55
Could temperate	27.34	34.00	24.41	33.12	31.68	26.19	31.55
Plateau temperate	35.08	66.01	48.53	48.33	60.07	49.95	42.85
Plateau frigid	8.59	13.98	10.93	9.46	11.35	9.20	9.22
Total	1252.46	1470.84	889.35	1602.05	1341.28	1025.40	1491.65

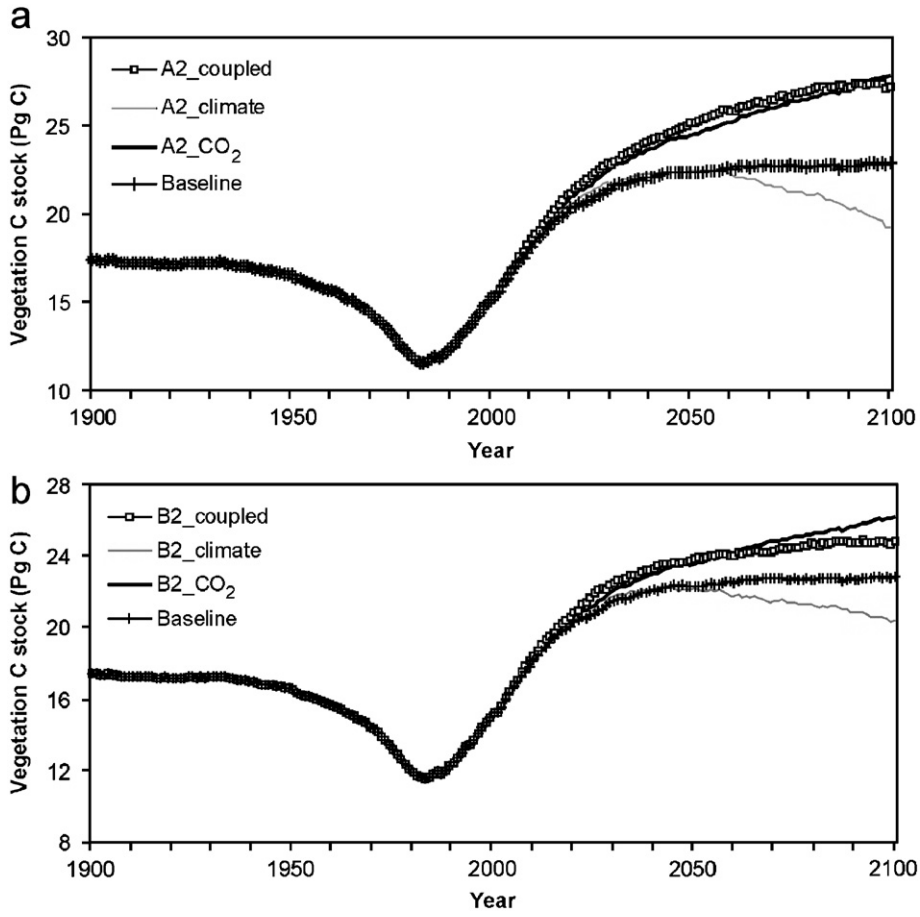

Fig. 7. Time series of simulated total vegetation carbon storage in China's forests under different climate change and increasing CO_2 scenarios. All simulations were driven by the same spatial and historical climate data sets and produced the same vegetation carbon storage for the period from 1901 to 2001. The difference in vegetation carbon storage during 2002–2100 is due to different future climate and CO_2 concentration data sets used.

years is 7.7 Pg C. The smallest increase is for the CGCM2-A2 climate impact run, only 4.0 Pg C during 2001 to 2100 (compared with the increase of 10.9 Pg C in the baseline run). The accumulation of C in the baseline run is mainly due to stand age dynamics and external N input from atmospheric deposition to the forest ecosystems. Stand age structure and N deposition will likely play more important roles in determining future C accumulation of China's forests.

3.3. Future carbon balance of China's forests

China's forests are currently acting as a C sink (Fig. 10a). Forests in Southeast, the eastern parts of Southwest and Northeast China are the major contributor to this sink, with NEP of most forests in the range from 200 to 400 g C m^{-2} yr^{-1} in the 1990s. In this period, forests in the western part of Southwest China were small C sinks of around 100 g C m^{-2} yr^{-1}. There were also some C sources sporadically distributed across the country, depending on disturbance history. The average C balance of China's forests was -80.5 Tg C yr^{-1} in the 1980s and 189 Tg C yr^{-1} in the 1990s. The global net C uptake by terrestrial ecosystems was 200 ± 600 Tg C yr^{-1} and 1400 ± 700 Tg C yr^{-1} during these two decades (Prentice et al., 2001). China's forests contributed about 13% of the global total terrestrial C sink in the 1990s. The Chinese fossil fuel emission was about 1000 Tg C yr^{-1} in 2000 (Lal, 2004). China's forests offset about 19% of the national fossil fuel emissions. The net C uptake by China's forests will peak around 2020 and then will gradually decline mainly due to the change in forest stand age structure, which leads to a gradual decrease in NPP (Fig. 3) and a continuous increase in heterotrophic respiration. It will stabilize at the level of about 33.5 Tg C yr^{-1} during 2091–2100 without climate change and increase in CO_2 (Fig. 11). In this situation, forests in the most of Northeast and the part of Southeast China will become small C sources of about 50 g C m^{-2} yr^{-1} during 2091–2100. At that time, the majority of China's forests will be small C sinks of 0–100 g C m^{-2} yr^{-1}(Fig. 10e).

The increase in CO_2 will delay the decline of NEP (Fig. 11). It will enhance NEP to the same extent for all forests since the spatial variation of the effect of CO_2

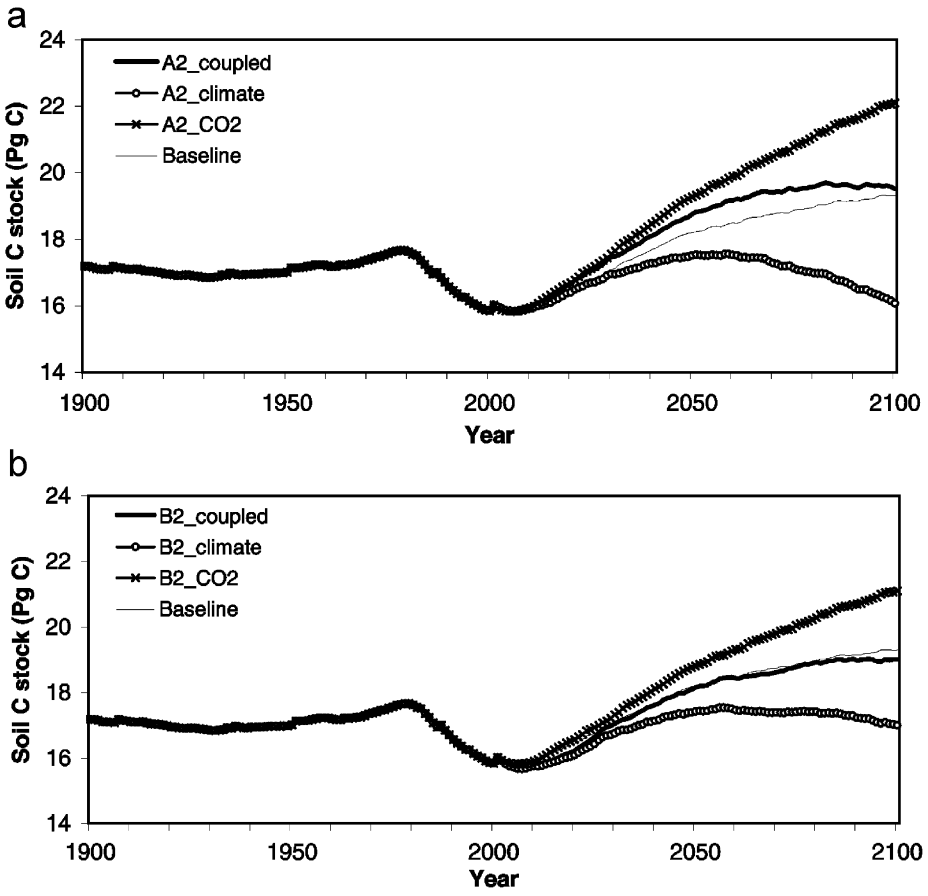

Fig. 8. Time series of simulated total soil carbon (including litter and soil organic carbon) storage in China's forests under different climate change and increasing CO_2 scenarios. All simulations were driven by same spatial and historical climate data sets and output same soil carbon storage during1901–2001. The difference in soil carbon storage during 2002–2100 is due to different future climate and CO_2 concentration data sets used.

fertilization is insignificant (Figs. 10c and g). Averaged over the period from 2001 to 2100, the increase in CO_2 will enhance NEP by 77.8 Tg C yr^{-1} and by 51.7 Tg C yr^{-1} under the CGCM2-A2 and -B2 CO_2 increase scenarios, respectively. This positive effect of the increase in CO_2 is still not large enough to offset the decline in NEP caused by the asymptote in NPP and the steady increase in heterotrophic respiration. With the increase in CO_2 alone, the majority of China's forests will be C sinks during 2091–2100, ranging from 0 to 100 g C m^{-2} yr^{-1}. Corresponding pure climate changes of CGCM2-A2 and -B2 alone will reduce NEP by 68.9 and 47.5 Tg C yr^{-1} averaged over the period from 2001 to 2100. The values of C sources during 2091–2100 are about 50 g C m^{-2} yr^{-1} under moderate warming of CGCM2-B2 and 50–200 g C m^{-2} yr^{-1} under warmer scenario of CGCM2-A2 (Figs. 10d and h). The climate-induced decrease in C sequestration will be mainly in subtropical climate zones (Table 5). For example, forests in the middle subtropical zone will absorb C at an average rate of 13.49 Tg C yr^{-1} during 2091–2100 without changes in climate and CO_2 concentration. Climate change alone will induce these forests to release C at the rate of 49.85 Tg C yr^{-1}. In cold temperate, plateau temperate, and plateau frigid zones, climate change will cause a small reduction in C sequestration by forests. In these areas, climate warming will significantly increase growing season length and consequently NPP. The large increase in NPP will partly offset the increase in heterotrophic respiration.

The combination of climate change and the increase in CO_2 produces less enhancement of NEP than the increase in CO_2 alone. The average NEP in 2001–2100 is 155.4 and 126.9 Tg C m^{-2} yr^{-1} in the CGCM2-A2 and -B2 coupled runs, respectively. The increases of NEP caused by the combined effect of these two factors are 45.3 and 16.8 Tg C yr^{-1}, respectively. In the CGCM2-A2 coupled run, China's forests will be a small C source of 7.6 Tg C yr^{-1} during 2091–2100, with most forests acting as C sources ranging from 0 to 40 g C m^{-2} yr^{-1}. In the coupled run of CGCM2-B2, China's forests will be a small C sink of 10.5 Tg C yr^{-1} during 2091–2100, with most forests acting as C sinks ranging from 0 to 40 g C m^{-2} yr^{-1} (Figs. 10b and f).

3.4. Sensitivity analysis of simulated NPP and NEP

A series of sensitivity experiments was carried out to analyze the uncertainty in simulated future C sequestration

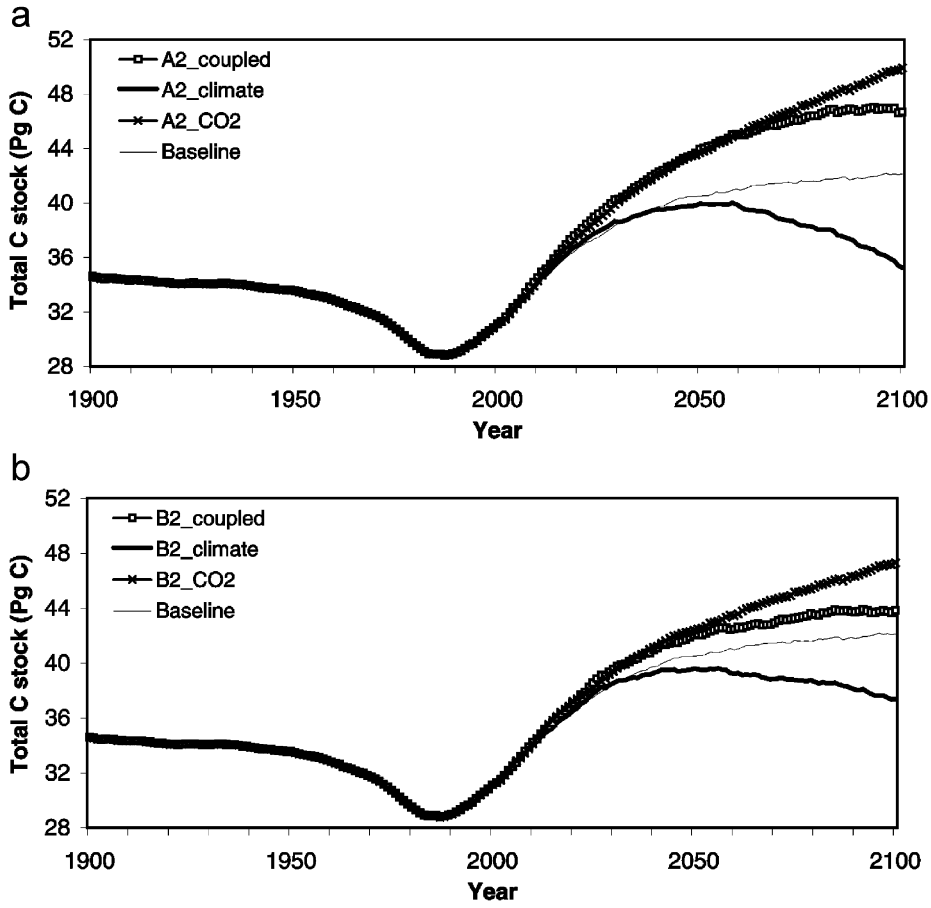

Fig. 9. Time series of simulated total carbon stock in China's forest ecosystems under different climate change and increasing CO_2 scenarios. All simulations were driven by same spatial and historical climate data sets and output same total carbon storage during1901–2001. The difference in total carbon storage during 2002–2100 is due to different future climate and CO_2 concentration data sets used.

of China's forests using the CGCM2-A2 coupled simulation as the baseline (Tables 4 and 5). In each of these simulations, one of the parameters affecting photosynthesis, N balance, or C decomposition was changed while inputs of climate and CO_2 concentration remained the same as those used in the CGCM2-A2 coupled run. The future C balance of China's forests is very sensitive to the Q_{10} value. If a Q_{10} value of 1.6 is used, NPP of China's forests will gradually increase during this century (Table 4) and China's forests will still act as a C sink of 66.9 Tg C yr^{-1} during 2091–2100. When a value of 3.0 is used for this parameter, China's forests will be a considerable C source of 103.7 Tg C yr^{-1} during 2091–2100 (compared to a source of 7.6 Tg C yr^{-1} in the base case of the CGCM2-A1 coupled run). This indicates the importance of properly representing the sensitivity of maintenance respiration in projecting the response of terrestrial C cycle to climate change. Terrestrial carbon models commonly used Q_{10} ranging from 2.0 to 2.3 (Raich et al., 1991; Bonan, 1995; Chen et al., 1999). A Q_{10} value of 2.3 used in this study is within this range. Recently, a change of Q_{10} with temperature has been implemented in some models (Arora, 2003), reflecting an apparent adaptation of vegetation to changing temperature that may yield a more realistic response of maintenance respiration. The future C sequestration of China's forests is also very sensitive to soil water availability. If average soil moisture in 1991–2000 is used for the period from 2002–2100, the NPP of China's forests will be 1652.0 Tg C yr^{-1} during 2091–2100, increasing by 181.6 Tg C yr^{-1} compared with the value in the CGCM2-A2 coupled run. Most of the increase in NPP is consumed by accelerated heterotrophic respiration. The NEP value will be only 34.5 Tg C yr^{-1}, 42.1 Tg C yr^{-1} larger than the result in the CGCM2-A2 coupled run. The future C sequestration of China's forests is less sensitive to N deposition scenario. When N deposition is fixed at the 2001 level, NPP is about 3% smaller in 2045–2054 and 2% smaller in 2091–2100 than for the base case (Table 6).

4. Conclusions

China's forests are currently acting as a C sink (189 Tg C yr^{-1} in the 1990s). This sink will peak around 2020

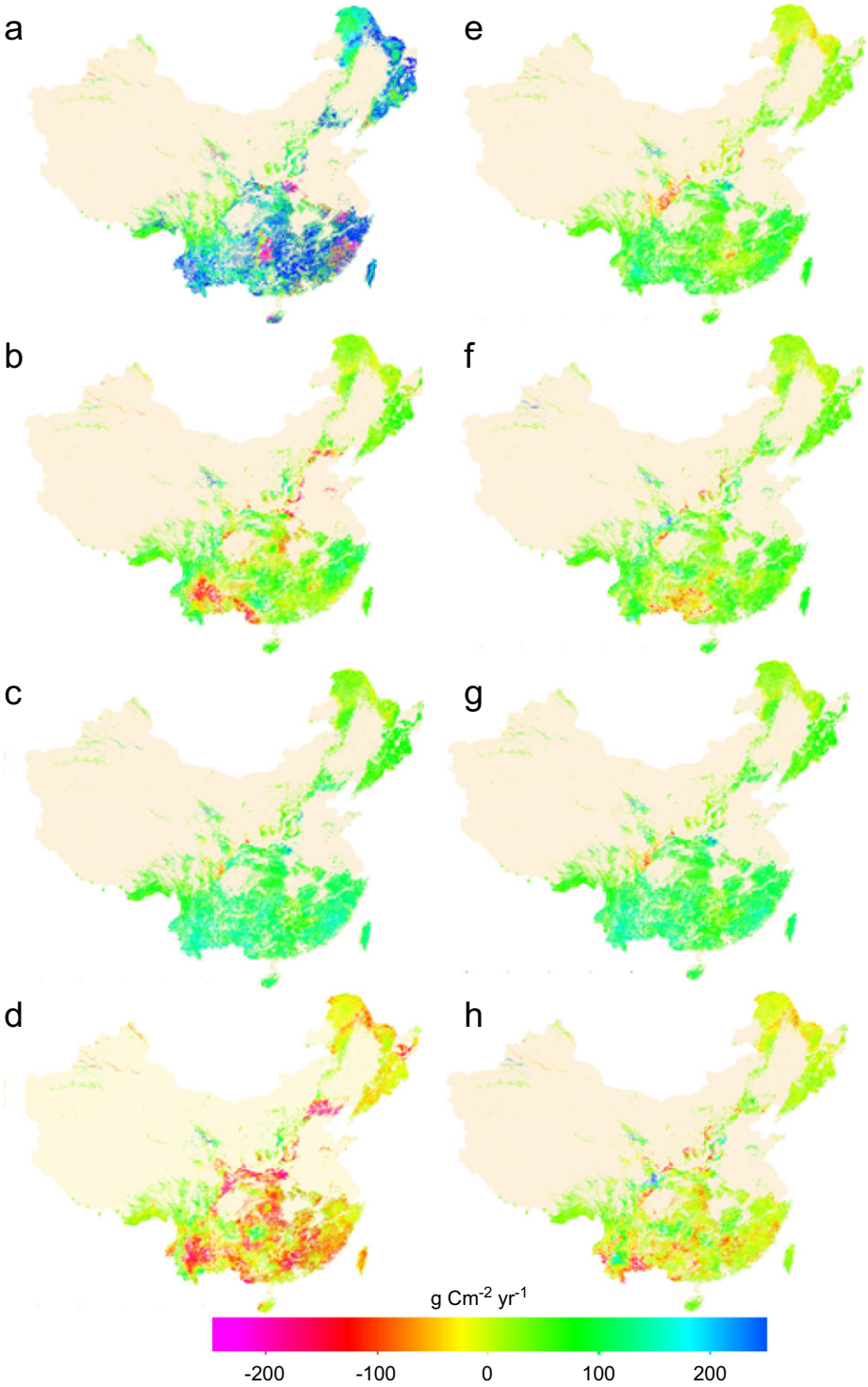

Fig. 10. Spatial distribution of carbon balance in China's forests: (a) during 1991–2000; (b)–(d) during 2091–2100 from the CGCM2-A2 coupled, CO_2 and climate impact runs, respectively; (e) during 2091–2100 from the baseline run; (f)–(h) during 2091–2100 from the CGCM2-B2 coupled, CO_2, and climate impact runs, respectively. Negative values are carbon sources, and vice versa.

and then gradually decline to 33.5 Tg C yr^{-1} during 2091–2100 without climate and CO_2 changes according to our simulations. The CGCM2 climate model projects that significant climate warming will occur in China in the 21th century and that the change in precipitation will be spatially heterogeneous. A series of modeling experiments is used to illustrate the joint and individual impacts of an increase in CO_2 and climate change on NPP, NEP, and long-term C accumulation in China forests.

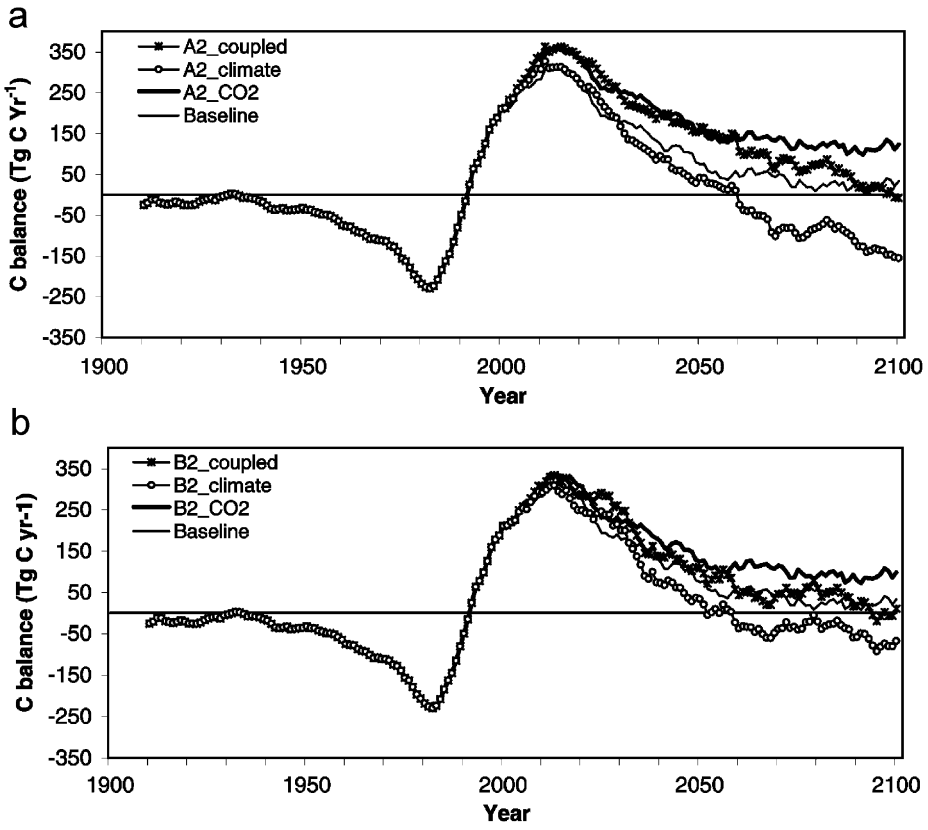

Fig. 11. Time series of simulated carbon balance in China's forest ecosystems under different climate change and increasing CO_2 scenarios. All simulations were driven by same spatial and historical climate data sets and output same results during1901–2001. After 2001, different future climate and CO_2 concentration data sets were used to drive the model.

Table 5
Simulated mean carbon balance of China's forests during 2091–2100 in different climate zones under different climate and CO_2 change scenarios (Tg C yr^{-1})

Climate zone	Simulations						
	Baseline	CGCM2-A2 coupled	CGCM2-A2 climate	CGCM2-A2 CO_2	CGCM2-B2 Coupled	CGCM2-B2 climate	CGCM2-B2 CO_2
Marginal tropical	2.00	1.53	−2.40	5.03	1.87	−2.36	4.31
Southern tropical	16.70	−8.03	−32.83	33.98	−1.63	−15.67	29.92
Middle tropical	13.49	−1.15	−49.85	45.65	1.04	−23.21	36.97
Northern tropical	8.29	0.94	−20.55	17.34	5.22	−4.37	14.80
Wet warm temperate	2.80	−3.22	−16.48	9.99	1.77	−4.64	7.69
Dry warm temperate	0.02	−0.03	−0.03	0.02	0.04	−0.01	0.01
Wet middle temperate	−7.22	−1.33	−22.81	5.36	−2.08	−14.19	2.25
Dry middle temperate	−0.20	−0.83	−4.40	1.47	1.10	−0.37	0.80
Could temperate	−2.08	−0.84	−3.71	−0.12	−1.13	−2.97	−0.58
Plateau temperate	−1.39	3.92	−1.99	3.25	3.37	−0.17	1.39
Plateau frigid	1.06	1.46	0.25	1.23	1.09	0.07	1.25
Total	33.47	−7.60	−154.80	123.19	10.65	−67.89	98.83

An increase in CO_2 always enhances the C uptake of China's forests. The values of the β factor are 0.35 and 0.42 in 2001–2100 for the CGCM2-A2 and -B2 CO_2 fertilization scenarios, smaller than those in some global studies. The simulated increase in NPP caused by CO_2 is also lower than the number derived in a FACE experiment. However, the enhancement of NPP by higher CO_2 tends to decline with time due to a decrease in N availability (Hungate

Table 6
Sensitivity analysis of simulated NPP and NEP (Tg C yr^{-1})

Simulations	NPP				NEP			
	2001–2100	2001–2010	2045–2054	2091–2100	2001–2100	2001–2010	2045–2054	2091–2100
Base case:								
$Q_{10} = 2.3$, changing N_{dep}, changing soil moisture, feedback between C/N ratios and C decomposition	1432.4	1274.2	1472.1	1470.5	155.4	339.3	148.3	−7.6
Sensitivity case:								
$Q_{10} = 1.6$, changing N_{dep}, changing soil moisture, feedback between C/N ratios and C decomposition	1461.1 (28.7)	1240.8 (−33.4)	1474.7 (2.6)	1630.6 (160.1)	169.7 (14.3)	309.4 (−29.9)	155.6 (7.3)	66.9 (74.5)
$Q_{10} = 3.0$, changing N_{dep}, changing soil moisture, feedback between C/N ratios and C decomposition	1343.6 (−88.8)	1278.1 (3.9)	1418.3 (−53.7)	1209.6 (−260.9)	119.9 (−35.6)	345.3 (6.0)	122.5 (−25.8)	−103.7 (−96.1)
$Q_{10} = 2.3$, fixed N_{dep} at the level of 2001, changing soil moisture, feedback between C/N ratios and C decomposition	1398.5 (−33.9)	1272.0 (−2.2)	1429.1 (−43.0)	1426.2 (−44.3)	144.9 (−106)	337.6 (−1.7)	130.2 (−18.1)	−10.1 (−2.5)
$Q_{10} = 2.3$, changing N_{dep}, average soil moisture of 1991–2000, feedback between C/N ratios and C decomposition	1518.9 (86.5)	1296.2 (22.0)	1535.8 (63.7)	1652.1 (181.6)	176.6 (21.2)	348.9 (9.7)	157.2 (8.9)	34.5 (42.1)

In all simulations, climate and CO_2 are same as those used in CGCM2-A2 coupled run. Only one of parameters in the table is changed in each simulation. Values in parenthesis are the departures from those in the CGCM2-A2 coupled run.

et al., 2003). The CO_2 fertilization effects on NPP by the end of this century are 349.6 and 241.7 Tg C yr^{-1} under CGCM2-A2 and -B2 increase scenarios, respectively. These effects increase by 199.1 and 126.6 Tg C yr^{-1} in the first 50 years, and thereafter, by 150.5 and 115.1 Tg C yr^{-1} in the second 50 years under CGCM2-A2 and -B2 increase scenarios, respectively. Under a CO_2 rise without climate change, the majority of China's forests will be C sinks during 2091–2100, ranging from 0 to 100 g C m^{-2} yr^{-1}.

Climate change will reduce the C sequestration of China's forests due to its negative effect on NPP and the enhancement of soil C decomposition. The reduction caused by climate change will mainly occur in the second half of this century. Without a corresponding increase in CO_2, China's forests would widely act as C sources during 2091–2100, releasing C to the atmosphere at the rates of about 50 g C m^{-2} yr^{-1} under the moderate warming of CGCM2-B2 and 50–200 g C m^{-2} yr^{-1} under the warmer scenario of CGCM2-A2, respectively.

The combination of an increase in CO_2 and climate change always has a larger positive effect on NPP and vegetation C stock than the increase in CO_2 alone during the first 50 years. After 2050, the negative effect of climate change will weaken the enhancement of NPP by the increase in CO_2. In the coupled run of CGCM2-A2, China's forests will be a small C source of 7.6 Tg C yr^{-1} during 2091–2100, with most forests acting as C sources with C balance ranging from 0 to −40 g C m^{-2} yr^{-1}. China's forests will be a small C sink of 10.5 Tg C yr^{-1} during 2091–2100, with most forests acting as C sinks ranging from 0 to 40 g C m^{-2} yr^{-1} under the CGCM2-B2 CO_2 and climate scenario.

The prediction of future C sequestration of China's forests is very sensitive to the Q_{10} value used to estimate the changing maintenance respiration, and to soil water availability, while being less sensitive to the N deposition scenario. In this study, the calculation of soil moisture is very simple and needs to be improved. Stand age structure has more important effects on C balance than climate change and the increase in CO_2. In this study, we do not consider the occurrence of future disturbances and the progressive increase in stand age after 2001, although we allow for progressive aging of the stand. This treatment inevitably introduces some errors in the temporal trends of simulated NPP and NEP, and may bias the results toward larger NPP and NEP than will occur in reality.

Acknowledgments

This research was funded by CIDA Project (Enhancing China's Forest Carbon Sequestration Capacity). We thank Dr. Xianfeng Feng for providing the reference NPP map of 2001. We gratefully acknowledge the constructive suggestions by three anonymous reviewers, which helped to improve the quality of manuscript greatly.

Appendix

A.1. Net biome productivity

$$\mathrm{NBP}(i) = \mathrm{NPP}(i) - R_{\mathrm{h}}(i) - R_{\mathrm{d}}(i) = \mathrm{NEP}(i) - R_{\mathrm{d}}(i), \tag{A.1}$$

where NBP(i) ($\mathrm{g\,C\,m^2\,yr^{-1}}$) is net biome productivity, NEP(i) ($\mathrm{g\,C\,m^2\,yr^{-1}}$) is net ecosystem productivity, NPP(i) ($\mathrm{g\,C\,m^2\,yr^{-1}}$) is net primary productivity, $R_{\mathrm{h}}(i)$ ($\mathrm{g\,C\,m^2\,yr^{-1}}$) is heterotrophic respiration, and $R_{\mathrm{d}}(i)$ ($\mathrm{g\,C\,m^2\,yr^{-1}}$) is direct emission of C to the atmosphere in the fired year, and i is the year number.

A.2. Direct emission of carbon to the atmosphere

The direct emission of C to the atmosphere $R_{\mathrm{d}}(i)$ is set to zero in nondisturbed years and estimated using a simplified model of Kasischke et al. (2000) in the disturbed year, i.e.,

$$R_{\mathrm{d}}(i) = C_{\mathrm{l}}(i) + 0.25C_{\mathrm{w}}(i) + C_{\mathrm{ssd}}(i) + C_{\mathrm{smd}}(i), \tag{A.2}$$

where $C_{\mathrm{l}}(i), C_{\mathrm{w}}(i), C_{\mathrm{ssd}}(i), C_{\mathrm{smd}}(i)$ ($\mathrm{g\,C\,m^2}$) are sizes of foliage, woody, surface structural, and surface metabolic litter C pools.

A.3. Heterotrophic respiration R_h

In the model, heterotrophic respiration is calculated using algorithms adopted from the CENTURY model. The model uses 9 pools to simulate soil C dynamics, i.e., (1) surface structural litter, (2) soil structural litter, (3) woody litter, (4) surface metabolic litter, (5) soil metabolic litter, (6) surface microbial, (7) soil microbial, (8) slow, and (9) passive C pools. Heterotrophic respiration is the sum of C released to the atmosphere during decomposition, i.e.

$$R_{\mathrm{h}}(i) = \sum_{j=1}^{9} k_{j,\mathrm{a}}(i)C_j(i), \tag{A.3}$$

where $k_{j,\mathrm{a}}(i)$ ($\mathrm{yr^{-1}}$) is the rate of C released from the jth C pool to the atmosphere, and $C_j(i)$ ($\mathrm{g\,C\,m^2}$) is the size of the jth C pool.

The decomposition rates of C pools are the products of maximum rates modified by soil temperature, moisture, texture, N availability, and lignin content (litter pools):

$$k_j(i) = \begin{cases} K_j KN_j(i)A(i)\mathrm{LC}_j, & j = 1,2,3, \\ K_j KN_j(i)A(i), & j = 4,5,8,9, \\ K_j A(i)T_{\mathrm{m}}, & j = 7, \\ K_j A(i), & j = 6, \end{cases} \tag{A.4}$$

where K_j ($\mathrm{yr^{-1}}$) is the maximum decomposition rate of the jth pool ($K_j = 3.9, 4.9, 2.4, 14.8, 18.5, 6.0, 7.3, 0.2, 0.0045\,\mathrm{yr^{-1}}$), $KN_j(i)$ (dimensionless) is the modifier for the effect of N availability on C decomposition, $A(i)$ (dimensionless) is the combined abiotic effect of soil temperature and moisture on soil C decomposition, T_{m} (dimensionless) is the effect of soil texture on soil microbial turnover, and LC_j (dimensionless) is the impact of lignin content on structural litter decomposition.

A.4. The abiotic effect on soil carbon decomposition

The annual value of abiotic effect is calculated as

$$A(i) = \frac{1}{12}\sum_{m-1}^{12} M_{\mathrm{s}}(i,m)T(i,m), \tag{A.5}$$

where $M_{\mathrm{s}}(i,m)$ (dimensionless) and $T(i,m)$ (dimensionless) are the scalars for the effects of soil moisture and temperature on decomposition in month m of year i, respectively. They are calculated as

$$M_{\mathrm{s}}(i,m) = 5.44\left(\frac{\theta(i,m)}{\theta_{\mathrm{S}}}\right) - 5.03\left(\frac{\theta(i,m)}{\theta_{\mathrm{s}}}\right)^2 - 0.472, \tag{A.6}$$

$$T(i,m) = \mathrm{e}^{308.56((1/(35+46.02))-(1/(T_s(i,m)+46.02)))}, \tag{A.7}$$

where $\theta(i,m)$ ($m^3\,m^{-3}$) and $T_s(i,m)$ (°C) are volumetric soil water content and soil temperature in month m of year i, and θ_s ($m^3\,m^{-3}$) is the soil porosity estimated from soil texture.

A.5. Balance of each carbon pool

The balance of each C pools is calculated as the difference between inputs and outputs. Annual NPP is allocated to four biomass C pools (foliage, woody, coarse root, and fine root) according to prescribed allocation coefficients for different cover types, i.e.

$$\Delta C_j(i) = (f_j\,\mathrm{NPP}(i) - k_j C_j(i))/(1+k_j), \tag{A.8}$$

where f_j (dimensionless) refers to the allocation coefficient of NPP to the jth biomass pool, and k_j (dimensionless) is the turn over rate of the jth biomass pool, which also depends on land cover type.

Soil carbon pools are updated as

$$\Delta C_j(i) = \left(\sum_{l=1}^{n} k_{l,j}(i) C_l(i-1) - k_j C_j(i-1))/(1+k_j\right), \tag{A.9}$$

where $k_{l,j}$ is the transfer rate of C from pool l to pool j, n is number of C pools transferring C to pool j, and k_j is the decomposition rate of pool j.

A.6. Calculation of NPP

Actual NPP of a forest is calculated as

$$\mathrm{NPP}(i) = \mathrm{NPP_u}(i)\mathrm{Fnpp}(i), \tag{A.10}$$

where $\mathrm{NPP_u}(i)$ is NPP value determined by nondisturbance factors (climate, CO_2, and N availability), Fnpp(i) is normalized forest productivity changing with age and it rages from 0 to 1.0, (Chen et al., 2000c).

Originally, the InTEC model assumes that the ratio of $\mathrm{NPP_u}$ to GPP is conservative with climate change and N status. This assumption possibly overestimates the positive effect of climate warming on NPP. To remove this limitation, NPP value of each year is progressively calculated using a modified method in this study, i.e.

$$\mathrm{NPP_u}(i) = \mathrm{GPP}(i) - R_a(i), \tag{A.11}$$

$$\mathrm{NPP_u}(i-1) = \mathrm{GPP}(i-1) - R_a(i-1), \tag{A.12}$$

$$\begin{aligned}\frac{\mathrm{NPP_u}(i) - \mathrm{NPP_u}(i-1)}{\mathrm{NPP_u}(i) + \mathrm{NPP_u}(i-1)} &= \frac{\mathrm{GPP}(i) - \mathrm{GPP}(i-1) - R_a(i) + R_a(i-1)}{\mathrm{GPP}(i) + \mathrm{GPP}(i-1) - R_a(i) - R_a(i-1)} \\ &= \frac{(X(i)-1) - \beta(i-1)(Y(i)-1)}{(X(i)+1) - \beta(i-1)(Y(i)+1)} = B(i).\end{aligned} \tag{A.13}$$

Therefore,

$$\mathrm{NPP_u}(i) = \mathrm{NPP_u}(i-1)\frac{1+B(i)}{1-B(i)}, \tag{A.14}$$

where $X(i)$ (dimensionless) is the interannual variability of GPP between year i and year $i-1$, which is calculated using modified InTEC model's approach, $\beta(i-1)$ (dimensionless) is the ratio of maintenance respiration to GPP in year $(i-1)$, and $Y(i)$ (dimensionless) is the interannual variability of maintenance respiration in year i and year $i-1$.

Maintenance respiration is calculated as

$$R_a(i) = (C_l R_{l,15} + C_s R_{s,15} + C_{cr} R_{cr,15} + C_{fr} R_{fr,15}) Q_{10}^{(T(i)-15/10)}, \tag{A.15}$$

where C_l,C_s, C_{cr}, and C_{fr} ($g\,C\,m^{-2}$) are respiratory C in foliage, woody (sapwood), coarse root, and fine root biomass pools, $R_{l,15}$ $R_{s,15}R_{cr,15}$, and $R_{fr,15}$ ($g\,C\,g^{-1}C\,yr^{-1}$) are annual respiration rates at an annual mean temperature of 15 °C, $T(i)$ (°C) is annual mean temperature in year i, and Q_{10} is the temperature sensitivity of maintenance respiration to temperature, a constant value of 2.3 used for all biomass pools. The interannual variability of maintenance respiration $Y(i)$ is

$$Y(i) = R_a(i)/R_a(i-1). \tag{A.16}$$

The ratio of maintenance respiration to GPP in the $(i-1)$th year $\beta(i-1)$ is calculated as

$$\beta(i-1)=\frac{R_a(i-1)}{\mathrm{NPP_u}(i-1)+R_a(i-1)}. \tag{A.17}$$

A.7. The variability of GPP

Canopy-level instant photosynthesis rate is calculated as

$$P_{can}=P_{can1}f_p+P_{can2}(1-f_p), \tag{A.18}$$

where P_{can1} and P_{can2} are canopy gross photosynthesis limited by electron transport and rubisco activity, respectively, and f_p is the fraction of canopy photosynthesis limited by P_{can1}.

Scaling up Farquhar's biochemical model from leaf to canopy, P_{can1} and P_{can2} are calculated as

$$P_{can1}=(J_{sun}L_{sun}+J_{shad}L_{shad})\frac{C_i-\Gamma}{4.5C_i+10.5\Gamma},\quad P_{can2}=V_m\frac{C_i-\Gamma}{C_i+k_{co}}L_t, \tag{A.19}$$

where L_t, L_{sun}, L_{shad} ($m^2\,m^{-2}$) are the total, sunlit , and shaded leaf area index, respectively; J, V_m, C_i, Γ, and k_{co} are calculated as (Bonan, 1995)

$$\begin{aligned}
J&=[J_m+0.38S-\sqrt{(J_m+0.38S)^2-1.064J_mS}]/1.4,\\
J_m&=J_{m25}\frac{N_l}{N_{l\,max}}a_{jm}^{(T_a-25)/10}/[1+e^{(85.4T_a-3147.7)/(T_a+273)}]=J_{m25}\frac{N_l}{N_{l\,max}}J_{mt},\\
V_m&=V_{m25}\frac{N_l}{N_{l\,max}}a_{vm}^{(T_a-25)/10}/[1+e^{(85.4T_a-3147.7)/(T_a+273)}]=V_{m25}\frac{N_l}{N_{l\,max}}V_{mt},\\
\Gamma&=40.2\times1.75^{(T_a-25)/10},k_{co}=300\times2.1^{(T_a-25)/10}+209\times1.75^{(T_a-25)/10},\\
C_i&=\alpha C_a,
\end{aligned} \tag{A.20}$$

where T_a (°C) is air temperature, S ($W\,m^{-2}$) is incoming solar radiation, N_l ($g\,N\,m^{-2}$) and $N_{l\,max}$ ($g\,N\,m^{-2}$) are actual and maximum leaf N content, V_{m25} (μmol $CO_2\,m^{-2}\,s^{-1}$) and J_{m25} (μmol $CO_2\,m^{-2}\,s^{-1}$) are carboxylation and electron transport rates at 25 °C, α is the ratio of intercellular CO_2 concentration to the atmospheric CO_2 concentration, determined by soil water availability, a_{jm} and a_{vm} are sensitivity of electron transport and rubisco activity to temperature, with values of 1.75 and 2.4, respectively, and C_a is atmospheric CO_2 concentration (ppmv).

The annual gross photosynthesis rate of a forest in year i is then given by integrating P_{can} over the time periods (growing season)

$$\mathrm{GPP}(i)=\int_t P_{can}(t)\,dt. \tag{A.21}$$

To reduce the requirement for data inputs and control the uncertainty in the calculation of historical photosynthesis, GPP(i) is calculated using a relationship between the interannual variability and the external forcing factors (Chen et al., 2000b):

$$\frac{d\mathrm{GPP}(i)}{di}=\int_t\frac{dP_{can}(t)}{di}\,dt+P_{can}(t)\frac{\partial l_g}{\partial i}, \tag{A.22}$$

where term I represents the effect on $\mathrm{GPP}(i)/di$ caused by changes in $P_{can}(t)$ and term II represents the effect caused by the change of growing season length (l_g).

From Eq. (A.22), interannual variability of annual photosynthesis rate is calculated using a temporal scaling algorithm developed by Chen et al. (2000b), i.e.

$$\frac{d\mathrm{GPP}(i)}{di}=\chi(i)\left[\frac{\mathrm{GPP}(i)+\mathrm{GPP}(i-1)}{2}\right] \tag{A.23}$$

and

$$\mathrm{GPP}(i)=\mathrm{GPP_u}(i-1)\frac{2+\chi(i)}{2-\chi(i)}=\mathrm{GPP_u}(i-1)X(i), \tag{A.24}$$

where $\chi(i)$ represents the integrated effect of climate, atmospheric CO_2 concentration, N, and soil water on annual photosynthesis and is given by

$$\begin{aligned}\chi(i) = \{&f_{\mathrm{p}}(i)[\xi_{L_{1,1}}\overline{L_{1,1}}(i)\Delta C_{\mathrm{a}} + \xi_{L_{2,1}}\overline{L_{2,1}}(i)\Delta\alpha + \xi_{L_{3,1}}\overline{L_{3,1}}(i)\Delta\Gamma + \xi_{L_{5,1}}\overline{L_{5,1}}(i)\Delta J_{\mathrm{mt}} \\ &+ \xi_{L_{N1}}\overline{L_{N1}}(i)\Delta N_l(i) + \xi_{L_{l1,1}}\overline{L_{L1,1}}(i)\Delta L_{\mathrm{sun}}(i) + \xi_{L_{l1,2}}\overline{L_{L1,2}}(i)\Delta L_{\mathrm{shad}}(i)] \\ &+ (1-f_{\mathrm{p}}(i))[\xi_{L_{1,2}}\overline{L_{1,2}}(i)\Delta C_{\mathrm{a}} + \xi_{L_{2,2}}\overline{L_{2,2}}(i)\Delta\alpha + \xi_{L_{3,2}}\overline{L_{3,2}}(i)\Delta\Gamma \\ &+ \xi_{L_{4,2}}\overline{L_{4,2}}(i)\Delta k_{\mathrm{co}} + \xi_{L_{5,2}}\overline{L_{5,2}}(i)\Delta V_{\mathrm{mt}} + \xi_{L_{N2}}\overline{L_{N2}}(i)\Delta N_{\mathrm{l}}(i)]\} + L_{\mathrm{g}}\,\Delta l_{\mathrm{g}},\end{aligned} \tag{A.25}$$

where Δ represents the interannual variability of a variable, ξ_{L_x} is a coefficient to correct the effects of diurnal and seasonal variations of L_x and P_{can} on $\mathrm{d}P$ and to correct the bias from the replacement of the temporal average of L_x by $\bar{L}_x$, which is calculated from mean values of environmental variables. Terms of $\bar{L}_x$ in Eq. (A.25) are defined as

$$\begin{aligned}\overline{L_{1,1}}(i) = 0.5\Bigg\{&\frac{15\overline{\alpha}(i)\overline{\Gamma}(i)}{[\overline{\alpha}(i)\overline{C_{\mathrm{a}}}(i) - \Gamma(i)][4.5\overline{\alpha}(i)\overline{C_{\mathrm{a}}}(i) + 10.5\overline{\Gamma}(i)]} \\ &+ \frac{15\overline{\alpha}(i-1)\overline{\Gamma}(i-1)}{[\overline{\alpha}(i-1)\overline{C_{\mathrm{a}}}(i-1) - \Gamma(i-1)][4.5\overline{\alpha}(i-1)\overline{C_{\mathrm{a}}}(i-1) + 10.5\overline{\Gamma}(i-1)]}\Bigg\},\end{aligned} \tag{A.26}$$

$$\begin{aligned}\overline{L_{2,1}}(i) = 0.5\Bigg\{&\frac{15\overline{C_{\mathrm{a}}}(i)\overline{\Gamma}(i)}{[\overline{\alpha}(i)\overline{C_{\mathrm{a}}}(i) - \Gamma(i)][4.5\overline{\alpha}(i)\overline{C_{\mathrm{a}}}(i) + 10.5\overline{\Gamma}(i)]} \\ &+ \frac{15\overline{C_{\mathrm{a}}}(i-1)\overline{\Gamma}(i-1)}{[\overline{\alpha}(i-1)\overline{C_{\mathrm{a}}}(i-1) - \Gamma(i-1)][4.5\overline{\alpha}(i-1)\overline{C_{\mathrm{a}}}(i-1) + 10.5\overline{\Gamma}(i-1)]}\Bigg\}\end{aligned} \tag{A.27}$$

$$\begin{aligned}\overline{L_{3,1}}(i) = \Bigg\{&\frac{15\overline{\alpha}(i)\overline{C_{\mathrm{a}}}(i)}{[\overline{\alpha}(i)\overline{C_{\mathrm{a}}}(i) - \Gamma(i)][4.5\overline{\alpha}(i)\overline{C_{\mathrm{a}}}(i) + 10.5\overline{\Gamma}(i)]} \\ &+ \frac{15\overline{\alpha}(i-1)\overline{C_{\mathrm{a}}}(i-1)}{[\overline{\alpha}(i-1)\overline{C_{\mathrm{a}}}(i-1) - \Gamma(i-1)][4.5\overline{\alpha}(i-1)\overline{C_{\mathrm{a}}}(i-1) + 10.5\overline{\Gamma}(i-1)]}\Bigg\},\end{aligned} \tag{A.28}$$

$$\begin{aligned}\overline{L_{5,1}} = 1/[\overline{J_{\mathrm{mt}}}(i) + \overline{J_{\mathrm{mt}}}(i-1)]\Bigg\{&\frac{\overline{J_{\mathrm{m}}}(i)\overline{L_{\mathrm{sun}}}(i)}{\overline{L_{\mathrm{t}}}(i)\overline{J}(i)}J_{T_{\mathrm{sun}}}(i) + \frac{\overline{J_{\mathrm{m}}}(i)\overline{L_{\mathrm{shade}}}(i)}{\overline{L_{\mathrm{t}}}(i)\overline{J}(i)}J_{T_{\mathrm{shade}}}(i) \\ &+ \frac{\overline{J_{\mathrm{m}}}(i-1)\overline{L_{\mathrm{sun}}}(i-1)}{\overline{L_{\mathrm{t}}}(i-1)\overline{J}(i-1)}J_{\mathrm{T}_{\mathrm{sun}}}(i-1) + \frac{\overline{J_{\mathrm{m}}}(i-1)\overline{L_{\mathrm{shade}}}(i-1)}{\overline{L_{\mathrm{t}}}(i-1)\overline{J}(i-1)}J_{T_{\mathrm{shade}}}(i-1)\Bigg\},\end{aligned} \tag{A.29}$$

$$J_{T_{\mathrm{sun}}}(i) = 0.714 - \frac{0.714\overline{J_{\mathrm{m}}}(i) - 0.1086\overline{S_{\mathrm{sun}}}}{\sqrt{(\overline{J_{\mathrm{m}}}(i) + 0.38\overline{S_{\mathrm{sun}}})^2 - 1.064\overline{J_{\mathrm{m}}}(i)\overline{S_{\mathrm{sun}}}}}, \tag{A.30}$$

$$J_{T_{\mathrm{shade}}}(i) = 0.714 - \frac{0.714\overline{J_{\mathrm{m}}}(i) - 0.1086\overline{S_{\mathrm{shade}}}}{\sqrt{(\overline{J_{\mathrm{m}}}(i) + 0.38\overline{S_{\mathrm{shade}}})^2 - 1.064\overline{J_{\mathrm{m}}}(i)\overline{S_{\mathrm{shade}}}}}, \tag{A.31}$$

$$\begin{aligned}\overline{L_{N,1}} = 1/[\overline{N_{\mathrm{l}}}(i) + \overline{N_{\mathrm{l}}}(i-1)]\Bigg\{&\frac{\overline{J_{\mathrm{m}}}(i)\overline{L_{\mathrm{sun}}}(i)}{\overline{L_{\mathrm{t}}}(i)\overline{J}(i)}J_{T_{\mathrm{sun}}}(i) + \frac{\overline{J_{\mathrm{m}}}(i)\overline{L_{\mathrm{shade}}}(i)}{\overline{L_{\mathrm{t}}}(i)\overline{J}(i)}J_{T_{\mathrm{shade}}}(i) \\ &+ \frac{\overline{J_{\mathrm{m}}}(i-1)\overline{L_{\mathrm{sun}}}(i-1)}{\overline{L_{\mathrm{t}}}(i-1)\overline{J}(i-1)}J_{T_{\mathrm{sun}}}(i-1) + \frac{\overline{J_{\mathrm{m}}}(i-1)\overline{L_{\mathrm{shade}}}(i-1)}{\overline{L_{\mathrm{t}}}(i-1)\overline{J}(i-1)}J_{T_{\mathrm{shade}}}(i-1)\Bigg\},\end{aligned} \tag{A.32}$$

$$L_{L1,1} = \left[\frac{\overline{J_{\mathrm{sun}}}(i)}{\overline{J}(i)} + \frac{\overline{J_{\mathrm{sun}}}(i-1)}{\bar{J}(i-1)}\right]\Big/[(\overline{L}(i) + \bar{L}(i-1)], \tag{A.33}$$

$$L_{L1,2} = \left[\frac{\overline{J_{\mathrm{shad}}}(i)}{\overline{J}(i)} + \frac{\overline{J_{\mathrm{shad}}}(i-1)}{\overline{J}(i-1)}\right]\Big/[(\overline{L}(i) + \overline{L}(i-1)], \tag{A.34}$$

$$\overline{L_{1,2}} = 0.5\left\{\frac{\overline{\alpha}(i)[\overline{K_{co}}(i)+\overline{\Gamma}(i)]}{[\overline{\alpha}(i)\overline{C_a}(i)-\overline{\Gamma}(i)][\overline{\alpha}(i)\overline{C_a}(i)+\overline{K_{co}}(i)]} + \frac{\overline{\alpha}(i-1)[\overline{K_{co}}(i-1)+\overline{\Gamma}(i-1)]}{[\overline{\alpha}(i-1)\overline{C_a}(i-1)-\overline{\Gamma}(i-1)][\overline{\alpha}(i-1)\overline{C_a}(i-1)+\overline{K_{co}}(i-1)]}\right\}, \tag{A.35}$$

$$\overline{L_{2,2}} = 0.5\left\{\frac{\overline{C_a}(i)[\overline{K_{co}}(i)+\overline{\Gamma}(i)]}{[\overline{\alpha}(i)\overline{C_a}(i)-\overline{\Gamma}(i)][\overline{\alpha}(i)\overline{C_a}(i)+\overline{K_{co}}(i)]} + \frac{\overline{C_a}(i-1)[\overline{K_{co}}(i-1)+\overline{\Gamma}(i-1)]}{[\overline{\alpha}(i-1)\overline{C_a}(i-1)-\overline{\Gamma}(i-1)][\overline{\alpha}(i-1)\overline{C_a}(i-1)+\overline{K_{co}}(i-1)]}\right\}, \tag{A.36}$$

$$\overline{L_{3,2}} = 0.5\left\{\frac{-1}{[\overline{\alpha}(i)\overline{C_a}(i)-\overline{\Gamma}(i)]} - \frac{1}{[\overline{\alpha}(i-1)\overline{C_a}(i-1)-\overline{\Gamma}(i-1)]}\right\}, \tag{A.37}$$

$$\overline{L_{4,2}} = 0.5\left\{\frac{-1}{[\overline{\alpha}(i)\overline{C_a}(i)+\overline{K_{co}}(i)]} - \frac{1}{[\overline{\alpha}(i-1)\overline{C_a}(i-1)+\overline{K_{co}}(i-1)]}\right\}, \tag{A.38}$$

$$\overline{L_{5,2}} = 0.5\left\{\frac{1}{\overline{V_m}(i)} + \frac{1}{\overline{V_m}(i-1)}\right\}, \tag{A.39}$$

$$\overline{L_{N,2}}(i) = \left[\frac{1}{\overline{N_l}(i)} + \frac{1}{\overline{N_l}(i-1)}\right], \tag{A.40}$$

$$L_g = \left[\frac{1}{l_g} + \frac{1}{l_g(i-1)}\right]. \tag{A.41}$$

Eqs. (A.25)–(A.41) are different from those used in previous versions of the InTEC model (Chen et al., 2000b). Originally, InTEC uses growing season mean temperature to calculate Γ,k_{co}, and V_m and to evaluate the temperature effect on annual GPP. The responses of Γ, k_{co}, and V_m to temperature are nonlinear. In this study, in order to give a reliable representation of the temperature effect on GPP, monthly mean temperature is first used to calculate Γ,k_{co}, and V_m for each month in the growing season. Then, averages of Γ,k_{co}, and V_m are then used to evaluated the interannual variability of GPP caused by the change in temperature. This new algorithm captures the effects of both interannual and seasonal variations of temperature on GPP.

A.8. Simulation of nitrogen cycle

N transformations among various litter and soil C pools follow C flows and equal to the product of the carbon flow and the CN ratios of the pools that receive the C. Nitrogen available for vegetation uptake is the sum of fixation N_{fix} deposition N_{dep}, net mineralization N_{min}.

N fixation is a function of temperature, precipitation, and microbial biomass:

$$N_{fix}(i) = c_1 2.0^{T_s(i)/10}\mathrm{APPT}(i)/0.45 \times (C_{sm}(i)+C_m(i))/200, \tag{A.42}$$

where c_1 (0.15 g N m^{-2} yr^{-1}) is coefficient determining fixation rate, $T_s(i)$ (°C) is annual mean soil temperature, APPT(i) (m) is annual precipitation, $C_{sm}(i)$ (g C m^{-2}) and $C_m(i)$ (g C m^{-2}) are the sizes of surface and soil microbial pools.

N deposition is interpolated for each year according to measurements of N deposition in a reference year i_{ref} (including dry and wet deposition), the increase rate of greenhouse gas emission:

$$N_{dep}(i) = N_{dep}(0) + \frac{[N_{dep}(i_{ref}) - N_{dep}(i_0)][G(i)-G(i_0)]}{G(i_{ref})-G(i_0)}, \tag{A.43}$$

where N_{dep} (g N m^{-2} yr^{-1}) is nitrogen deposition rate in year i, G (Tg C yr^{-1}) is greenhouse gas emission rate, i_0, i_{ref}, and i represent the initial, the reference, and a simulation years.

Net N mineralization depends on the C transfers and C/N ratios of all soils C pools:

$$\begin{aligned}N_{\min}(i) = {} & \frac{C_{\mathrm{ssd}}(i)(k_{\mathrm{ssd,sm}}+k_{\mathrm{ssd,s}}+k_{\mathrm{ssd,a}})}{CN_{\mathrm{ssd}}(i)}+\frac{C_{\mathrm{smd}}(i)(k_{\mathrm{smd,sm}}+k_{\mathrm{smd,a}})}{CN_{\mathrm{smd}}(i)}\\ & +\frac{C_{\mathrm{fsd}}(i)(k_{\mathrm{fsd,m}}+k_{\mathrm{fsd,s}}+k_{\mathrm{fsd,a}})}{CN_{\mathrm{fsd}}(i)}+\frac{C_{\mathrm{fmd}}(i)(k_{\mathrm{fmd,m}}+k_{\mathrm{fmd,a}})}{CN_{\mathrm{fmd}}(i)}\\ & +\frac{C_{\mathrm{cd}}(i)(k_{\mathrm{cd,m}}+k_{\mathrm{cd,s}}+k_{\mathrm{cd,a}})}{CN_{\mathrm{cd}}(i)}+\frac{C_{\mathrm{sm}}(i)(k_{\mathrm{sm,s}}+k_{\mathrm{sm,a}})}{CN_{\mathrm{sm}}(i)}\\ & +\frac{C_{\mathrm{m}}(i)(k_{\mathrm{m,s}}+k_{\mathrm{m,p}}+k_{\mathrm{m,a}})}{CN_{\mathrm{m}}(i)}+\frac{C_{\mathrm{s}}(i)(k_{\mathrm{s,m}}+k_{\mathrm{s,p}}+k_{\mathrm{s,a}})}{CN_{\mathrm{s}}(i)}\\ & +\frac{C_{\mathrm{p}}(i)(k_{\mathrm{p,m}}+k_{\mathrm{p,s}}+k_{\mathrm{p,a}})}{CN_{p}(i)}-\frac{C_{\mathrm{ssd}}(i)k_{\mathrm{sd,sm}}+C_{\mathrm{smd,sm}}(i)k_{\mathrm{smd,sm}}}{CN_{sm}(i)}-\frac{C_{\mathrm{s}}(i)k_{\mathrm{s,p}}+C_{\mathrm{m}}(i)k_{\mathrm{m,p}}}{CN_{p}(i)}\\ & -\frac{C_{\mathrm{fsd}}(i)k_{\mathrm{fsd,m}}+C_{\mathrm{fmd}}(i)k_{\mathrm{fmd,m}}+C_{\mathrm{cd}}(i)k_{\mathrm{cd,m}}+C_{\mathrm{s}}(i)k_{\mathrm{s,m}}+C_{\mathrm{p}}(i)k_{\mathrm{p,m}}}{CN_{m}(i)}\\ & -\frac{C_{\mathrm{fsd}}(i)k_{\mathrm{fsd,s}}+C_{\mathrm{fmd}}(i)k_{\mathrm{fmd,s}}+C_{\mathrm{cd}}(i)k_{\mathrm{cd,s}}+C_{\mathrm{m}}(i)k_{\mathrm{m,s}}+C_{\mathrm{p}}(i)k_{\mathrm{p,s}}}{CN_{\mathrm{s}}(i)}.\end{aligned} \tag{A.44}$$

The amount of N available $N_{\mathrm{av}}(i)$ ($\mathrm{g\,N\,m^{-2}}$) for forest uptake is the total of N fixation, deposition and net mineralization:

$$N_{\mathrm{av}}(i) = N_{\mathrm{fix}}(i)+N_{\mathrm{dep}}(i)+N_{\min}(i). \tag{A.45}$$

N uptake by forest $N_{\mathrm{up}}(i)$ ($\mathrm{g\,N\,m^{-2}}$) is determined by N availability, fine root mass $C_{\mathrm{fr}}(i)$, i.e.

$$N_{\mathrm{up}}(i) = \frac{N_{\mathrm{av}}(i)}{1+bN_{\mathrm{av}}(i)/C_{\mathrm{fr}}(i)}, \tag{A.46}$$

where b is a coefficient determining the maximum uptake capacity of a forest (Chen et al., 2000b):

$$N_{\mathrm{l}}(i) = C_{\mathrm{l}}(i)/CN_{\mathrm{l}}(i)/L, \tag{A.47}$$

where $N_{\mathrm{l}}(i)$ is leaf nitrogen content ($\mathrm{g\,N\,m^{-2}}$), $CN_{\mathrm{l}}(i)$ is the ratio of C to N in leaves, L is total leaf area.

The C/N ratios of surface and soil microbial C pools are fixed at 12 while other C pools have fluctuated C/N ratios:

$$\begin{aligned}CN_{\mathrm{l}}(i) = {} & [(1-K_{\mathrm{l}})C_{\mathrm{l}}(i-1)+f_{\mathrm{l}}\,\mathrm{NPP}(i-1)]\Big/\left[\frac{(1-K_{\mathrm{l}})C_{\mathrm{l}}(i-1)}{CN_{\mathrm{l}}(i-1)}+\frac{f_{\mathrm{l}}}{CN_{\mathrm{l}}(i-1)}\right.\\ & \left.\times\frac{N_{\mathrm{up}}(i)}{f_{\mathrm{l}}/CN_{\mathrm{l}}(i-1)+f_{\mathrm{fr}}/CN_{\mathrm{fr}}(i-1)+(f_{\mathrm{w}}+f_{\mathrm{cr}})/CN_{\mathrm{w}}(i-1)}\right],\end{aligned} \tag{A.48}$$

$$\begin{aligned}CN_{\mathrm{fr}}(i) = {} & [(1-K_{\mathrm{fr}})C_{\mathrm{fr}}(i-1)+f_{\mathrm{fr}}\,\mathrm{NPP}(i-1)]\Big/\left[\frac{(1-K_{\mathrm{fr}})C_{\mathrm{fr}}(i-1)}{CN_{\mathrm{fr}}(i-1)}+\frac{f_{\mathrm{fr}}}{CN_{\mathrm{fr}}(i-1)}\right.\\ & \left.\times\frac{N_{\mathrm{up}}(i)}{f_{\mathrm{l}}/CN_{\mathrm{l}}(i-1)+f_{\mathrm{fr}}/CN_{\mathrm{fr}}(i-1)+(f_{\mathrm{w}}+f_{\mathrm{cr}})/CN_{\mathrm{w}}(i-1)}\right],\end{aligned} \tag{A.49}$$

$$\begin{aligned}CN_{\mathrm{w}}(i) = {} & [C_{\mathrm{w}}(i-1)+C_{\mathrm{cr}}(i-1)+(f_{\mathrm{w}}+f_{\mathrm{cr}})\mathrm{NPP}(i-1)]\Big/\left[\frac{C_{\mathrm{w}}(i-1)+C_{\mathrm{cr}}(i-1)}{CN_{\mathrm{w}}(i-1)}+\frac{f_{\mathrm{w}}+f_{\mathrm{cr}}}{CN_{\mathrm{w}}(i-1)}\right.\\ & \left.\times\frac{N_{\mathrm{up}}(i)}{f_{\mathrm{l}}/CN_{\mathrm{l}}(i-1)+f_{\mathrm{fr}}/CN_{\mathrm{fr}}(i-1)+(f_{\mathrm{w}}+f_{\mathrm{cr}})/CN_{\mathrm{w}}(i-1)}\right],\end{aligned} \tag{A.50}$$

$$CN_{\mathrm{cd}}(i) = C_{\mathrm{cd}}(i)\Big/\left[\frac{C_{\mathrm{cd}}(i-1)}{CN_{\mathrm{cd}}(i-1)}+\frac{K_{\mathrm{w,cd}}C_{\mathrm{w}}(i)+K_{\mathrm{cr,cd}}C_{\mathrm{crr}}(i)}{CN_{\mathrm{w}}(i)}-\frac{C_{\mathrm{cd}}(i-1)(K_{\mathrm{cd\_m}}+K_{\mathrm{cd\_s}}+K_{\mathrm{cd\_a}})}{CN_{\mathrm{cd}}(i-1)}\right], \tag{A.51}$$

$$CN_{\mathrm{ssd}}(i) = C_{\mathrm{ssd}}(i)\Big/\left[\frac{C_{\mathrm{ssd}}(i-1)}{CN_{\mathrm{ssd}}(i-1)}+\frac{K_{l}C_{l}(i)(1-F_{\mathrm{m}}(i))}{CN_{l}(i)}-\frac{C_{\mathrm{ssd}}(i-1)(K_{\mathrm{ssd,sm}}+K_{\mathrm{ssd,s}}+K_{\mathrm{ssd,a}})}{CN_{\mathrm{ssd}}(i-1)}\right], \tag{A.52}$$

$$CN_{\mathrm{smd}}(i) = C_{\mathrm{smd}}(i)\Big/\left[\frac{C_{\mathrm{smd}}(i-1)}{CN_{\mathrm{smd}}(i-1)}+\frac{K_{1}C_{1}(i-1)F_{\mathrm{m}}(t)}{CN_{\mathrm{l}}(i)}-\frac{C_{\mathrm{smd}}(i-1)(K_{\mathrm{smd,sm}}+K_{\mathrm{smd,a}})}{CN_{\mathrm{smd}}(t-1)}\right], \tag{A.53}$$

$$CN_{\mathrm{fsd}}(i) = C_{\mathrm{fsd}}(i) \Big/ \left[\frac{C_{\mathrm{fsd}}(i-1)}{CN_{\mathrm{fsd}}(i-1)} + \frac{K_{\mathrm{fr}} C_{\mathrm{fr}}(i)(1 - F_{\mathrm{m}}(i))}{CN_{\mathrm{fr}}(i)} - \frac{C_{\mathrm{fsd}}(i-1)(K_{\mathrm{fsd,m}} + K_{\mathrm{fsd,s}} + K_{\mathrm{fsd,a}})}{CN_{\mathrm{fsd}}(i-1)} \right], \tag{A.54}$$

$$CN_{\mathrm{fmd}}(i) = C_{\mathrm{fmd}}(i) \Big/ \left[\frac{C_{\mathrm{fmd}}(i-1)}{CN_{\mathrm{fmd}}(i-1)} + \frac{K_{\mathrm{fr}} C_{\mathrm{fr}}(i) F_{\mathrm{m}}(i)}{CN_{\mathrm{fr}}(i)} - \frac{C_{\mathrm{fmd}}(i-1)(K_{\mathrm{fmd,m}} + K_{\mathrm{fmd,a}})}{CN_{\mathrm{fmd}}(i-1)} \right], \tag{A.55}$$

$$\begin{aligned} CN_{\mathrm{s}}(i) = C_{\mathrm{s}}(t) \Big/ \Bigg[& \frac{C_{\mathrm{s}}(i-1)}{CN_{\mathrm{s}}(i-1)} + \frac{K_{\mathrm{ssd,s}} C_{\mathrm{ssd}}(i-1)}{CN_{\mathrm{ssd}}(i)} + \frac{K_{\mathrm{fsd,s}} C_{\mathrm{fsd}}(i-1)}{CN_{\mathrm{fsd}}(i)} + \frac{K_{\mathrm{cd,s}} C_{\mathrm{cd}}(i-1)}{CN_{\mathrm{cd}}(i)} \\ & + \frac{K_{\mathrm{m,s}} C_{\mathrm{m}}(i-1)}{CN_{\mathrm{m}}(i)} + \frac{K_{\mathrm{sm,s}} C_{\mathrm{sm}}(i-1)}{CN_{\mathrm{sm}}(i)} - \frac{C_{\mathrm{s}}(i-1)(K_{\mathrm{s,m}} + K_{\mathrm{s,p}} + K_{\mathrm{s,a}})}{CN_{\mathrm{s}}(i-1)} \Bigg], \end{aligned} \tag{A.56}$$

$$CN_{\mathrm{p}}(i) = C_{\mathrm{p}}(i) \Big/ \left[\frac{C_{\mathrm{p}}(i-1)}{CN_{\mathrm{p}}(i-1)} + \frac{K_{\mathrm{s,p}} C_{\mathrm{s}}(i-1)}{CN_{\mathrm{s}}(i-1)} + \frac{K_{\mathrm{m,p}} C_{\mathrm{m}}(i-1)}{12.0} - \frac{C_{\mathrm{p}}(t-1)(K_{\mathrm{p,m}} + K_{\mathrm{p,a}})}{CN_{\mathrm{p}}(t-1)} \right], \tag{A.57}$$

$$F_{\mathrm{m}}(i) = 0.85 - 0.6 \times 0.018 \times [CN_{\mathrm{l}}(i) + CN_{\mathrm{fr}}(i)]. \tag{A.58}$$

A.9. The effect of nitrogen on carbon decomposition

N availability has feedbacks on C decomposition through two mechanisms. The C/N ratios of foliage and fine root C pools determine the fractions of foliage and fine root litter partitioned into structural and metabolic pools. Foliage and fine root litters with low C/N ratios will transfer more into metabolic C pools, which have higher decomposition rates than structural C pools. The decomposition of soil C pools is regulated by N availability.

The N flow during the decomposition of a C pool j is computed as

$$\mathrm{NAV}_j(i) = \hat{K}_j(i) C_j(i) / CN_j(i) - \sum_{l=1}^{n} \frac{\hat{K}_{j,\mathrm{l}}(i) C_j(i)}{CN_{\mathrm{l}}(i)}, \tag{A.59}$$

where $\mathrm{NAV}_j(i)$ ($\mathrm{g\,N\,m^{-2}\,yr^{-1}}$) represents the potentially mineralized (or immobilized) N in the decomposition of pool j, and $\hat{K}_j(i)$ (dimensionless) is the decomposition rate of C pool j without N limitation.

The N balance β ($\mathrm{g\,N\,m^{-2}\,yr^{-1}}$) is given as

$$\beta(i) = N_{\mathrm{fix}}(i) + N_{\mathrm{dep}}(i) + \sum_{j=1}^{9} \mathrm{NAV}_j(i). \tag{A.60}$$

If $\beta(i) < 0$, the system is N-limited, the extent to which the decomposition rates of various C pools are reduced as

$$N_{\mathrm{sup}}(i) = N_{\mathrm{fix}}(i) + N_{\mathrm{dep}}(i) + \sum_{j=1}^{9} \mathrm{NAV}_j(i) \quad \mathrm{NAV}_j(i) > 0, \tag{A.61}$$

$$N_{\mathrm{need}}(i) = \sum_{j=1}^{9} \left| \mathrm{NAV}_j(i) \right| \quad \mathrm{NAV}_j(i) < 0, \tag{A.62}$$

$$KN_j(i) = \begin{cases} \dfrac{N_{\mathrm{sup}}(i)}{N_{\mathrm{need}}(i)} & \text{if } \mathrm{NAV}_i(i) < 0, \\ 1 & \text{else.} \end{cases} \tag{A.63}$$

A.10. Relative canopy conductivity to CO_2

The mean of intercellular CO_2 concentration $C_i(i)$ in the growing season (May to September) ith year is calculated as

$$C_i(i) = \frac{1}{5} \sum_{m=5}^{9} \alpha(i, m) C_{\mathrm{a}}(i), \tag{A.64}$$

where $\alpha(i,m)$ is a dimensionless multiplier accounting for the change of canopy conductivity to CO_2 related to soil moisture availability, ranging from 0 to 1.0. Following the TEM model (Pan et al., 1998), $\alpha(i,m)$ is computed as

$$\alpha(i,m)=\begin{cases}0.1+0.9\dfrac{\mathrm{AET}(i,m)}{\mathrm{PET}(i,m)}, & \dfrac{\mathrm{AET}(i,m)}{\mathrm{PET}(i,m)}>0.1,\\ -10\left(\dfrac{\mathrm{AET}(i,m)}{\mathrm{PET}(i,m)}\right)^2+2.9\dfrac{\mathrm{AET}(i,m)}{\mathrm{PET}(i,m)}, & \dfrac{\mathrm{AET}(i,m)}{\mathrm{PET}(i,m)}\leqslant 0.1,\end{cases} \tag{A.65}$$

where AET(i,m) (m) and PET(i,m) (m) are potential and actual evapotranspiration in month m of year i, respectively.

A.11. Calculations of PET and AET

Following Romanenko (1961), monthly potential evapotranspiration PET(i,m) (m) is calculated as

$$\mathrm{PET}(i,m)=\begin{cases}0.19[1-r(i,m)][20+T(i,m)]^2/1000 & \text{if } T(i,m)>0,\\ 0 & \text{else,}\end{cases} \tag{A.66}$$

where r (%) is monthly mean of humidity and $T(i,m)$ (°C)is monthly mean air temperature.

Monthly AET (mm) is the lesser of supply and demand:

$$\mathrm{AET}(i,m)=\begin{cases}\min\{I(i,m)+[\mathrm{PET}(i,m)-I(i,m)]R(i,m), I(i,m)+[\theta(i,m-1)-WP]\} & \text{if } I(i,m)<\mathrm{PET}(i,m),\\ \mathrm{PET}(i,m) & \text{else,}\end{cases} \tag{A.67}$$

where $I(i,m)$ (m) is the total water infiltration during the month (rainfall and snowfall if applicable), $R(i,m)$ is the relative drying rate scalar for potential water extraction as a function of soil moisture (defined in (A.69)), $\theta(i,m-1)$ is the volumetric soil moisture content in the $(t-1)$th month, and WP is the wilting point determined from soil texture with soil water potential equal to 1500 kPa. AET is computed 4 times within each monthly time step in a prediction-correction numerical integration.

For months with monthly mean temperature $\leqslant 0$ °C, PET(i,m) and AET(i,m) are set to zero and there is no change in soil water content. During these months, precipitation goes into the snow pack, which is added to $I(i,m)$ in the first month when monthly average air temperature is above 0 °C.

The soil water content is calculated using a bucket nonlinear drying soil water balance model with soil rooting depth set to 1 m. For each month with temperature above 0 °C, soil moisture is updated in terms of water infiltration, PET(i,m), and $R(i,m)$. If monthly water infiltration $I(i,m)$ exceeds PET(i,m), the surface soil moisture content is increased and excessive soil water above the field capacity is treated as runoff to leave the system. On the contrary, if $I(i,m)$ is insufficient to meet the demand of PET(i,m), the plant consumes the totality of $I(i,m)$ and a fraction of the pre-existing soil water:

$$\theta(i,m)=\begin{cases}\theta(i,m-1)-R(i,m)[\mathrm{PET}(i,m)-I(i,m)] & \text{if } I(i,m)<\mathrm{PET}(i,m),\\ \theta(i,m-1)+[I(i,m)-\mathrm{PET}(i,m)] & \text{else,}\\ \min(\theta(i,m),\mathrm{FC}) & \end{cases} \tag{A.68}$$

where FC is the field capacity determined from soil texture with soil water potential equal to 10 kPa for sandy soils and 33 kPa for clay soils.

The relative drying rate scalar $R(i,m)$ in (A.67) and (A.68) is given by

$$R(i,m)=\begin{cases}1 & \text{if } \theta(i,m-1)\geqslant \mathrm{FC},\\ [\theta(i,m-1)-\mathrm{WP})/(\mathrm{FC}-\mathrm{WP}) & \text{if } \mathrm{WP}<\theta(i,m-1)<\mathrm{FC},\\ 0 & \text{if } \theta(i,m-1)<\mathrm{WP}.\end{cases} \tag{A.69}$$

References

Alexandrov, G.A., Oikawa, T., Yamagata, Y., 2003. Climate dependence of the CO_2 fertilization effect on terrestrial net primary production. Tellus B 55, 669–675.

Anthony, W.K., Wilerred, M.P., Stan, D.W., 1997. The potential response of terrestrial carbon storage to changes in climate and atmospheric CO_2. Climatic Change 35, 199–227.

Apps, M.J., Bahatti, J.S., Halliwell, D., Jiang, H., 2000. Influence of uniform versus random disturbance regime on carbon dynamics in the

boreal forest of central Canada. In: Global Change and Cold Ecosystems. CRC Press, Boca Raton, FL, pp. 413–426.
Arora, V.K., 2003. Simulating energy and carbon fluxes over winter wheat using coupled land surface and terrestrial ecosystem models. Agricultural and Forest Meteorology 118, 21–47.
Barr, A.G., Griffis, T.J., Black, T.A., Lee, X., Staebler, R.M., Fuentes, J.D., Chen, Z., Morgenstern, K., 2002. Comparing the carbon budgets of boreal and temperate deciduous forest stands. Canadian Journal of Forest Research 32, 813–822.
Berthelot, M., Friedlingstein, P., Ciais, P., Monfray, P., Dufresne, J.L., Le Treut, H., Fairhead, L., 2002. Global response of the terrestrial biosphere to CO_2 and climate change using a coupled climate–carbon cycle model. Global Biogeochemical Cycles 16 (4), 1084, doi:10.1029/2001GB001827.
Black, T.A., Chen, W.J., Barr, A.G., Arain, M.A., Chen, Z., Nesic, Z., Hogg, E.H., Neumann, H.H., Yang, P.C., 2000. Increased carbon sequestration by a boreal deciduous forest in years with a warm spring. Geophysical Research Letters 27, 1271–1274.
Bonan, G.B., 1995. Land-atmosphere CO_2 exchange simulated by a land surface process model coupled to an atmospheric general circulation model. Journal of Geophysical Research 100 (D2), 2817–2831.
Cao, M.K., Woodward, F.I., 1998. Net primary and ecosystem production and carbon stocks of terrestrial ecosystems and their responses to climate change. Global Change Biology 4, 185–198.
Cao, M.K., Prince, S.D., Li, K.R., Tao, B., Small, J., Shao, X.M., 2003. Response of terrestrial carbon uptake to climate interannual variability in China. Global Change Biology 9, 536–546.
Chen, J.M., Liu, J., Cihlar, J., Goulden, M.L., 1999. Daily canopy photosynthesis model through temporal and spatial scaling for remote sensing applications. Ecological Modelling 124, 99–119.
Chen, J., Chen, W.J., Liu, J., Cihlar, J., Gray, S., 2000a. Annual carbon balance of Canada's forests during 1895–1996. Global Biogeochemical Cycles 14, 839–849.
Chen, W.J., Chen, J., Cihlar, J., 2000b. An integrated terrestrial ecosystem carbon-budget model based on changes in disturbance, climate, and atmospheric chemistry. Ecological Modelling 135, 55–79.
Chen, W.J., Chen, J., Liu, J., Cihlar, J., 2000c. Approaches for reducing uncertainties in regional forest carbon balance. Global Biogeochemical Cycles 14, 827–838.
Chen, J.M., Ju, W.M., Cihlar, J., Price, D., Liu, J., Chen, W.J., Pan, J.J., Black, A., Barr, A., 2003. Spatial distribution of carbon sources and sinks in Canada's forests. Tellus B 55, 622–641.
Cotrufo, M.F., Ineson, P., 1996. Elevated CO_2 reduces field decomposition rates of *Betula pendula* (Roth) leaf litter. Oecologia 106, 525–530.
Cramer, W., Bondeau, A., Woodward, F.I., Prentice, I.C., Betts, R.A., Brovkin, V., Cox, P.M., Fisher, V., Foley, J.A., Friend, A.D., Kucharik, C., Lomas, M.R., Ramankutty, N., Sitch, S., Smith, B., White, A., Young-Molling, C., 2001. Global response of terrestrial ecosystem structure and function to CO_2 and climate change: results from six dynamic global vegetation models. Global Change Biology 7, 357–373.
Fang, J.Y., Chen, A.P., Peng, C.H., Zhao, S.Q., Ci, L., 2001. Changes in forest biomass carbon storage in China between 1949 and 1998. Science 292, 2320–2322.
Fang, J.Y., Piao, S., Field, C.B., Pan, Y., Guo, Q.H., Zhou, L.M., Peng, C.H., Tao, S., 2003. Increasing net primary production in China from 1982 to 1999. Frontiers in Ecology and the Environment 1, 293–297.
Feng, X.F., Liu, G.H., Chen, J.M., Chen, M.Z., Liu, J., Ju, W.M., Sun, R., Zhou, W., 2006. Net primary productivity of China's terrestrial ecosystems from a process model driven by remote sensing. Journal of Environmental Management, (this issue), doi:10.1016/j.jenvman.2006.09.021.
Flato, G.M., Boer, G.J., 2001. Warming asymmetry in climate change simulations. Geophysical Research Letters 28, 195–198.
Giorgi, F., Hewiston, B., Christensen, J., Hulme, M., Von Storch, H., Whetton, P., Jones, R., Mearns, L., Fu, C., 2001. Regional climate information-evaluation and projections. In: Houghton, J.T., Ding, Y., Griggs, D.J., Noguer, M., van der Linden, P.J., Dai, X., Maskell, K., Johnson, C.A. (Eds.), Climate Change 2001: The Scientific Basis. Contribution of Working Group I to the Third Assessment Report of the Intergovernmental Panel on Climate Change. Cambridge University Press, Cambridge, UK.
Gough, W.A., Leung, A., 2002. Nature and fate of Hudson Bay permafrost. Regional Environmental Change 2, 177–184.
Gower, S.T., Mcmurtrie, R.E., Murty, D., 1996. Aboveground net primary production decline with stand age: potential causes. Trends in Ecology & Evolution 11, 378–382.
Griffis, T.J., Black, T.A., Morgenstern, K., Barr, A.G., Nesic, Z., Drewitt, G.B., Gaumont-Guay, D., Mccaughey, J.H., 2003. Ecophysiological controls on the carbon balances of three southern boreal forests. Agricultural and Forest Meteorology 117, 53–71.
Hungate, B.A., Dukes, J.S., Shaw, M.R., Luo, Y., Field, C.B., 2003. Nitrogen and climate change. Science 302, 1512–1514.
Jarvis, P.G., 1976. Interpretation of variations in leaf water potential and stomatal conductance found in canopies in field. Philosophical Transactions of the Royal Society of London Series B 273, 593–610.
Johnson, D.W., Cheng, W., Ball, J.T., 2000. Effects of CO_2 and N fertilization on decomposition and N immobilization in ponderosa pine litter. Plant and Soil 224, 115–122.
Ju, W.M., Chen, J.M., 2005. Distribution of soil carbon stocks in Canada's forests and wetlands simulated based on drainage class, topography and remotely sensed vegetation parameters. Hydrological Processes 19, 77–94.
Ju, W.M., Chen, J.M., Black, T.A., Barr, A.G., McCaughey, H., Roulet, N.T., 2006. Hydrological effects on C cycles of Canada's forests and wetlands. Tellus B 50B, 16–30.
Kasischke, E.S., O'Neill, K.P., French, N.H.F., Bourgeau-Chavez, L.L., 2000. Controls on patterns of biomass burning in Alaska boreal forests. In: Kasischke, E.S., Stocks, B.J. (Eds.), Fire, Climate Change and Carbon Cycling in the Boreal Forest. Springer, New York.
King, A.W., Post, W.M., Wullschleger, S.D., 1997. The potential response of terrestrial carbon storage to changes in climate and atmospheric CO_2. Climatic Change 35, 199–227.
Lal, R., 2004. Offsetting China's CO_2 emissions by soil carbon sequestration. Climatic Change 65, 263–275.
Lal, R., 2005. Forest soils and carbon sequestration. Forest Ecology and Management 220, 242–258.
Liu, J., Chen, J.M., Cihlar, J., Chen, W., 2002. Net primary productivity mapped for Canada at 1-Km resolution. Global Ecology and Biogeography 11, 115–129.
Ludeke, M.K.B., Donges, S., Otto, R.D., Kindermann, J., Badeck, F.W., Ramge, P., Jakel, U., Kohlmaier, G.H., 1995. Responses in NPP and carbon stores of the northern biomes to a CO_2-induced climatic change, as evaluated by the Frankfurt biosphere model (FBM). Tellus B 47, 191–205.
Marissink, M., Pettersson, R., Sindhoj, E., 2002. Above-ground plant production under elevated carbon dioxide in a Swedish semi-natural grassland. Agriculture Ecosystems and Environment 93, 107–120.
New, M., Hulme, M., Jones, P., 1999. Representing twentieth-century space-time climate variability. Part I: development of a 1961–90 mean monthly terrestrial climatology. Journal of Climate 12, 829–856.
New, M., Hulme, M., Jones, P., 2000. Representing twentieth-century space-time climate variability. Part II: development of 1901–96 monthly grids of terrestrial surface climate. Journal of Climate 13, 2217–2238.
Ni, J., 2000. Net primary production, carbon storage and climate change in Chinese biomes. Nordic Journal of Botany 20, 415–426.
Norby, R.J., Delucia, E.H., Gielen, B., Calfapietra, C., Giardian, C.P., King, J.S., Ledford, J., et al., 2005. Forest response to elevated CO_2 is conserved across a broad rang of productivity. Proceedings of the National Academy of Sciences of the United States of America 102 (50), 18052–18056.
Oren, R., Ellsworth, D.S., Johnsen, K.H., Phillips, N., Ewers, B.E., Maier, C., Schafer, K.V.R., Mccarthy, H., Hendrey, G., Mcnulty, S.G., Katul, G.G., 2001. Soil fertility limits carbon sequestration by forest ecosystems in a CO_2-enriched atmosphere. Nature 411, 469–472.

Pan, Y.D., Melillo, J.M., Mcguire, A.D., Kicklighter, D.W., Pitelka, L.F., Hibbard, K., Pierce, L.L., Running, S.W., Ojima, D.S., Parton, W.J., Schimel, D.S., 1998. Modeled responses of terrestrial ecosystems to elevated atmospheric CO_2: a comparison of simulations by the biogeochemistry models of the vegetation/ecosystem modeling and analysis project (VEMAP). Oecologia 114, 389–404.

Pan, Y., Luo, T., Hom, J., Melillo, J., 2004. New estimates of carbon storage and sequestration in China's forests: effects of age-class and method on inventory-based carbon estimation. Climatic Change 67, 211–236.

Parton, W.J., Schimel, D.S., Cole, C.V., Ojima, D.S., 1987. Analysis of factors controlling soil organic matter levels in great plains grasslands. Soil Science Society of America Journal 51, 1173–1179.

Peltoniemi, M., Makipaa, R., Liski, J., Tamminen, P., 2004. Changes in soil carbon with stand age—an evaluation of a modelling method with empirical data. Global Change Biology 10, 2078–2091.

Potter, C.S., Randerson, J.T., Field, C.B., Matson, P.A., Vitousek, P.M., Mooney, H.A., Klooster, S.A., 1993. Terrestrial ecosystem production—a process model-based on global satellite and surface data. Global Biogeochemical Cycles 7, 811–841.

Prentice, I.C., Farquhar, G.D., Fasham, M.J.R., Golden, M.L., Heiman, M., Jaramillo, V.J., Kheshgi, H.S., Quéré, C.L.e., Scholes, R.J., Wallace, D.W.R., 2001. The carbon cycle and atmospheric carbon dioxide. In: Houghton, J.T., Ding, Y., Griggs, D.J., Noguer, M., van der Linden, P.J., Dai, X., Maskell, K., Johnson, C.A. (Eds.), Climate Change 2001: the Scientific Basis. Contribution of Working Group I to the Third Assessment Report of the Intergovernmental Panel on Climate Change. Cambridge University Press, Cambridge, UK.

Raich, J.W., Rastetter, J.W., Melillo, J.M., Kicklighter, D.K., Steudler, P.A., Peterson, B.J., 1991. Potential net primary productivity in south America: application of a global model. Ecological Application 1 (4), 399–429.

Rapalee, G., Trumbore, S.E., Davidson, E.A., Harden, J.W., Veldhuis, H., 1998. Soil carbon stocks and their rates of accumulation and loss in a boreal forest landscape. Global Biogeochemical Cycles 12, 687–701.

Rasse, D.P., Peresta, G., Drake, B.G., 2005. Seventeen years of elevated CO_2 exposure in a Chesapeake Bay Wetland: sustained but contrasting responses of plant growth and CO_2 uptake. Global Change Biology 11, 369–377.

Romanenko, V.A., 1961. Computation of the autumn soil moisture using a universal relationship for a large area. In: Proceedings Ukrainian Hydrometeorological Research Institute (Kiev) 3.

Sadowsky, M.J., Schortemeyer, M., 1997. Soil microbial response to increased concentration of atmospheric CO_2. Global Change Biology 3, 217–224.

Shao, Y.H., Pan, J.J., Yang, L.X., Chen, J.M., Ju, W.M., Shi, X.Z., 2006. Tests of soil organic carbon density modeled by InTEC in China's forest ecosystems. Journal of Environmental Management (this issue), doi:10.1016/j.jenvman.2006.09.006.

Sun, O.J., Campbell, J., Law, B.E., Wolf, V., 2004. Dynamics of carbon stocks in soils and detritus across chronosequences of different forest types in the Pacific Northwest, USA. Global Change Biology 10, 1470–1481.

Torn, M.S., Trumbore, S.E., Chadwick, O.A., Vitousek, P.M., Hendricks, D.M., 1997. Mineral control of soil organic carbon storage and turnover. Nature 389, 170–173.

Tricker, P.J., Trewin, H., Kull, O., Clarkson, G.J.J., Eensalu, E., Tallis, M.J., Colella, A., Doncaster, C.P., Sabatti, M., Taylor, G., 2005. Stomatal conductance and not stomatal density determines the long-term reduction in leaf transpiration of poplar in elevated CO_2. Oecologia 143, 652–660.

Turunen, J., Roulet, N.T., Moore, T.R., Richard, P.J.H., 2004. Nitrogen deposition and increased carbon accumulation in ombrotrophic peatlands in eastern Canada. Global Biogeochemical Cycles 18, GB3002.

Wang, C.K., Bond-Lamberty, B., Gower, S.T., 2003. Carbon distribution of a well- and poorly-drained black spruce fire chronosequence. Global Change Biology 9, 1066–1079.

Wang, S., Huang, M., Shao, X., Mickler, R.A., Li, K., Li, J., 2004. Vertical distribution of soil organic carbon in China. Environmental Management 33 (Supplement 1), 200–209.

Wang, S., Chen, J.M., Ju, W.M., Feng, X.F., Chen, M.Z., Chen, P.Q., Yu, G.R., 2006. Carbon sinks and sources of China's forests during 1901–2001. Journal of Environmental Management, (this issue), doi:10.1016/j.jenvman.2006.09.019.

White, A., Cannell, M.G.R., Friend, A.D., 2000. The high-latitude terrestrial carbon sink: a model analysis. Global Change Biology 6, 227–245.

Yang, L.X., Pan, J.J., Shao, Y.H., Yuan, S.F., 2006. Soil organic carbon decomposition and carbon pools in temperate and sub-tropical forests in China. Journal of Environmental Management (this issue), doi:10.1016/j.jenvman.2006.09.011.